Atmos. Chem. Phys. Discuss., 14, 9849–9901, 2014
www.atmos-chem-phys-discuss.net/14/9849/2014/
doi:10.5194/acpd-14-9849-2014

Atmospheric Chemistry and Physics Discussions

Enhancements of the refractory submicron aerosol fraction in the Arctic polar vortex: feature or exception?

R. Weigel[1], C. M. Volk[2], K. Kandler[3], E. Hösen[2,*], G. Günther[4], B. Vogel[4], J.-U. Grooß[4], S. Khaykin[5,], G. V. Belyaev[6], and S. Borrmann[1,7]**

[1]Institut für Physik der Atmosphäre, Johannes Gutenberg-Universität, Mainz, Germany
[2]Department of Physics, University of Wuppertal, Germany
[3]Institut für Angewandte Geowissenschaften, Technische Universität Darmstadt, Germany
[4]Institut für Energie- und Klimaforschung (IEK-7), Forschungszentrum Jülich, Germany
[5]Central Aerological Observatory, Dolgoprudny, Moskow Region, Russia
[6]Myasishchev Design Bureau, Zhukovsky-5, Moscow Region, Russia
[7]Partikelchemie, Max-Planck-Institut für Chemie, Mainz, Germany
[*]now at: Institut für Ozeanographie, Universität Hamburg, Germany
[**]now at: CNRS/INSU, LATMOS-IPSL, Université de Versailles St. Quentin, Guyancourt, France

Received: 31 March 2014 – Accepted: 6 April 2014 – Published: 16 April 2014

Correspondence to: R. Weigel (weigelr@uni-mainz.de)

Published by Copernicus Publications on behalf of the European Geosciences Union.

ACPD
14, 9849–9901, 2014

Abstract

In situ measurements with a 4-channel stratospheric condensation particle counter (CPC) were conducted at up to 20 km altitude on board the aircraft M-55 *Geophysica* from Kiruna, Sweden, in January through March (EUPLEX 2003; RECONCILE 2010) and in December (ESSenCe, 2011). During all campaigns air masses from the upper stratosphere and mesosphere were subsiding inside the Arctic winter vortex, thus transporting refractory aerosol into the lower stratosphere ($\Theta < 500$ K) by vertical dispersion. The strength and extent of this downward transport varied between the years depending on the dynamical evolution of the vortex. Inside the vortex and at altitudes of potential temperatures $\Theta \geq 450$ K as many as eight of eleven particles per cm^3 contained refractory material, thermally stable residuals with diameters from 10 nm to a few µm which endure heat exposure of 250 °C. Particle mixing ratios (up to 150 refractory particles per milligram of air) and fractions of non-volatile particles (up to 75 % of totally detected particles) reach highest values in air masses with lowest content of nitrous oxide (N_2O, down to 70 nmol mol^{-1}). This indicates that refractory aerosol originates from the upper stratosphere or the mesosphere. From mixing ratios of the long lived tracer N_2O (simultaneously measured in situ) an empirical index was derived which serves to differentiate air masses according to their origin from inside the vortex, the vortex edge region, and outside the vortex. Previously, observed high fractions of refractory submicron aerosol in the 2003 Arctic vortex were ascribed to unusually strong subsidence during that winter. Measurements under perturbed vortex conditions in 2010 and during early winter in December 2011, however, revealed similarly high values. Thus, the abundance of refractory aerosol at high levels appears to be a feature rather than the exception for the Arctic vortices. During December, the import from aloft into the lower stratosphere appears to be developing; thereafter the abundance of refractory aerosol inside the vortex reaches its highest levels until March. A measurement-based estimate of the total mass of refractory aerosol inside the vortex is provided for each campaign. Based on the derived increase of particle mass in the lower stratospheric

ACPD
14, 9849–9901, 2014

vortex (100–67 hPa pressure altitude) on the order of 32×10^6 kg between early and late winter and assuming a mesospheric origin, we estimate the total mass of mesospheric particles deposited in the Arctic vortex and compare it to the expected atmospheric influx of meteoritic material ($110 \pm 55 \times 10^3$ kg per day). Such estimates at present still hold considerable uncertainties which are discussed in detail. Nevertheless, the results strongly suggest that the Arctic vortex easily achieves the drainage of all meteoric material deposited on the upper atmosphere.

1 Introduction

In situ measurements of the aerosol vertical distribution inside the Arctic winter vortex of the year 1989 revealed an increase of the mixing ratios of sub-micrometer sized particles with altitude (Wilson et al., 1990). Also in the Arctic (from Kiruna, Northern Sweden), in the year 2003, similar vertical profiles were observed (Curtius et al., 2005) and it could be shown that an increase of particle concentrations coincided with an increasing fraction of non-volatile aerosol compounds. Both studies demonstrated that the abundance of particles is closely linked to air mass subsidence inside the vortex from upper stratospheric or mesospheric altitudes down to the Arctic lower stratosphere. Such particles provide surfaces for heterogeneous reactions and deposition of condensable gases. Thus, their presence in the polar winter stratosphere may play a crucial role in formation of polar stratospheric clouds (PSC) (Voigt et al., 2005; Hoyle et al., 2013; Engel et al., 2013) or in heterogeneous chemistry (Peter, 1997; Solomon, 1999; Peter and Grooß, 2012) connected to ozone depletion. A downward import of non-volatile particles potentially occurring on a regular basis inside the vortex could imply an important natural process linked to atmospheric ozone chemistry.

The major import of refractory aerosol material into the upper atmosphere is expected to occur with the entry of micrometeorites (with particle diameter d_p below 1 mm), particularly of interplanetary dust particles (IDPs; $d_p < 1\,\mu$m), and by the ablation of meteoroids penetrating the atmosphere (von Zahn, 2005). Results from single

ACPD
14, 9849–9901, 2014

particle chemical analyses in the UT/LS (Upper Troposphere/Lowermost Stratosphere) at mid-latitudes and in the tropics of aerosols with diameters between 300 nm and about 1 µm suggest meteoritic ablation material to be included in a large fraction of stratospheric particles (Murphy, 2013, and reference therein). The total mass flux of meteoritic material into the atmosphere is estimated by various studies with different approaches. These estimates range from less than 20×10^3 kg per day (Plane, 2004) to fluxes between 20×10^3 kg and 100×10^3 kg per day (Cziczo et al., 2001; Gabrielli et al., 2004) and to $110 \pm 55 \times 10^3$ kg per day (Love and Brownlee, 1993; Peucker-Ehrenbrink, 1996). The last value currently seems to be the most accepted according to detailed discussions by von Zahn, 2005.

A certain fraction of this total daily influx is assumed to experience little or no ablation because the meteoritic bodies are too small. With a mass below 10^{-11} kg their sizes usually are smaller than 20 µm in diameter (Jones and Kaiser, 1966) and such small objects are not sufficiently heated by friction with atmospheric air molecules when entering the atmosphere. For large meteoroid masses, e.g. above 100×10^3 kg and size larger than 4 m in diameter the number of atmosphere hitting events (about one per year; von Zahn, 2005) is too small to significantly contribute to the total influx of meteoritic material. Furthermore von Zahn, 2005, estimated that those bodies entering the atmosphere which are in the mass range of 10^{-11} to 10^{-5} kg (approximately corresponding to size diameters between 20 µm and 2 mm) contribute the bulk part of the total influx. They are nearly fully vaporized at altitudes of about 100 km (von Zahn, 2005), providing a source of many smaller, long-lived particles, either from fragments, ablation smoke or from recondensation of vaporized meteoritic material. Experimental studies provided evidence for the presence of meteoritic ablation material in the mesosphere (Rapp et al., 2007; Rapp and Strelnikova, 2009; Strelnikova et al., 2009). The size of these particles may range from clusters of molecules with diameters of about 1 nm to a few hundreds of nanometers. This size distribution of secondary cosmic aerosols overlaps with the size distribution of IDPs that enter the atmosphere without strong thermal alteration. As a result, the size distribution of refractory aerosol in the

ACPD
14, 9849–9901, 2014

upper atmosphere is expected to be restricted to the particle diameter range of 1 nm to 20 µm. Particularly in the lower range ($d_p < 1$ µm) the particles have atmospheric residence times of several months to years. Once these particles enter regions with saturated vapors, for example of H_2SO_4, HNO_3 or H_2O, it is plausible that heterogeneous condensation leads to particle coating and growth and, finally, their removal due to increased sedimentation speed or, at some point, even incorporation in clouds.

The stratospheric vortex development causes large scale subsidence of air masses in the polar region during winter. As this downward transport drives an import of non-volatile particles from altitudes of the upper stratosphere or mesosphere (Curtius et al., 2005), it is commonly assumed that the non-volatile particles to a large extent originate from space. Other studies (e.g. Randall et al., 2006; Vogel et al., 2008) related to the Arctic polar vortex show that also NO_x-rich air masses from the upper stratosphere and mesosphere, caused by energetic particle precipitation (EPP) or solar proton events (SPEs), are transported downward in a strong, well-isolated vortex. These studies support the hypothesis that the polar vortex could act as major driver for downward transport of air masses from the mesosphere and upper stratosphere. Hence, the polar vortex could act as a major drain pathway of meteoritic aerosol from the upper stratosphere and mesosphere towards the UT/LS, followed by material removal onto the Earth's surface.

If the subsidence of refractory particles was a regular feature, this could play an important role for heterogeneous polar stratospheric cloud (PSC) formation as the particles provide surfaces for condensation (cf. Hoyle et al., 2013; Engel et al., 2013; Molleker et al., 2014). This would be the case particularly in times of relative volcanic quiescence where relatively low particle concentrations in the stratospheric Junge aerosol layer are reached as for example in 1997 (i.e. six years after the Mt. Pinatubo eruption; Borrmann et al., 2000). Whether such particles are involved in other microphysical processes, like triggering heterogeneous freezing, seems plausible but remains unclear despite the results from bulk freezing experiments by Biermann et al., 1996. PSCs promote denitrification of the polar lower stratosphere as demonstrated

ACPD
14, 9849–9901, 2014

for the RECONCILE winter by Grooß et al., 2014; Woiwode et al., 2014, and Molleker et al., 2014. Denitrification essentially contributes to ozone loss in the polar winter stratosphere (Fahey et al., 1990; Mann et al., 2003; Waibel et al., 1999). If the subsidence of refractory aerosol depends on the vortex being undisturbed as the winter progresses, the number of refractory aerosol particles in the Arctic lower stratosphere will increase with time. In this case, the abundance of surfaces available for condensation processes and PSC formation along with denitrification also increases over the course of the winter season.

In this study we address the question whether the observed import of refractory particles into the Arctic lower stratosphere due to the vortex subsidence was an exceptional event in 2003 (Curtius et al., 2005; Engel et al., 2006) or rather a feature that occurs more frequently in Arctic winters. Also we derive parameterizations of the vertical distribution of refractory aerosol within the vortex for the three campaigns which may be suitable for example for numerical simulations of heterogeneous PSC formation. Finally, we estimate how much the total refractory aerosol mass – as extrapolated from our in situ measurements within the vortex – corresponds to the northern hemispheric daily mass influx of meteoritic material. This way it might be possible to clarify whether the Arctic vortex is an important pathway for draining parts of the daily imported meteoritic material from the upper atmosphere.

2 Instruments and methods

2.1 Submicron particles

Aerosol concentrations were measured by using a 4-channel continuous flow condensation particle counter COPAS (COndensation PArticle counting System) using a chlorofluorocarbon (FC-43) as working liquid. COPAS measurements and data storage occur at 1 Hz frequency. Three of the four COPAS channels operate with different 50 % detection particle diameters d_{p50} (i.e. 6, 10 and 15 nm; with N_{10} denoting the

ACPD
14, 9849–9901, 2014

mixing ratio for the particles with diameters larger than 10 nm up to a few µm) while the fourth COPAS channel (with d_{p50} = 10 nm) counts aerosol particles after they passed a heated sample flow line resulting in measured particle mixing ratios of non-volatile (nv) particles, N_{10}nv. At an operational temperature of 250 °C and over the pressure range 70–300 hPa this aerosol pre-heater volatilizes more than 98 % of H_2SO_4-H_2O particles (Weigel et al., 2009) such that the detector channel downstream of the heated sample flow line exclusively accounts for refractory residuals (e.g. soot, mineral dust, metallic aerosol material, etc.).

The entry of the forward facing aerosol sample inlet of COPAS is positioned well outside of the aircraft boundary layer and it consists of two serial diffusors decelerating the air from the free flow to pumping velocity at near-isokinetic conditions. The COPAS measurement uncertainty is about 10 % for stratospheric particle concentrations based on particle counting statistics and uncertainties in the volume flow. The COPAS measurement characteristics are described in detail by Weigel et al., 2009, and its performance is demonstrated by several studies (Curtius et al., 2005; Borrmann et al., 2010; Frey et al., 2011; Weigel et al., 2011).

Particle concentrations are initially measured in particle number per cubic centimeter of sampled air but here provided as mixing ratio N in units of particles per milligram of air (mg^{-1}) for comparing measurements from different pressure altitudes and for correlations with tracer mixing ratios. The fraction f of non-volatile particles is given as the ratio of N_{10}nv and N_{10} in % because only non-volatile particles with sizes $d_p > 10$ nm are detected. The measurement of particles with $d_p > 6$ nm and $d_p > 15$ nm aims in principle at the identification of recently occurred new particle formation (NPF, cf. Weigel et al., 2011). However, throughout all measurements discussed here, no such event was identified.

2.2 Dynamic tracer nitrous oxide

Nitrous Oxide (N_2O), a long lived atmospheric tracer, is measured in situ on board the M-55 *Geophysica* by the HAGAR (High Altitude Gas AnalyzeR) instrument as

ACPD
14, 9849–9901, 2014

described by Werner et al., 2010, and Homan et al., 2010. N_2O is measured by gas chromatography with electron capture detection (GC/ECD) along with other long-lived species like chlorofluorocarbons (CFCs), sulfur hexafluoride (SF_6) and methane (CH_4) with a temporal resolution of 90 s. The mean precision for the N_2O measurements given in % of the tropospheric value (~ 320 ppb) is below 0.5 % for all three campaigns, except the first four flights during EUPLEX (for which it is 1–1.3 %). For most flights it is in fact below 0.3 %.

N_2O is generated at the surface and has its sink at high altitudes, generally above the tropopause as the N_2O molecules are increasingly destroyed with altitude by UV-photo-dissociation and reaction with oxygen. Thus, air masses with low N_2O mixing ratio originate from high altitude, i.e. in the mid to upper stratosphere or mesosphere.

HAGAR measurements of the N_2O mixing ratio along with potential temperature additionally allow for deriving a so-called ΔN_2O vortex index (ξ_{vi}), an empirical measure essentially obtained by linearly rescaling N_2O mixing ratios at a given time and potential temperature to vortex index values of $\xi_{vi} = 1$ inside the vortex and $\xi_{vi} = 0$ at mid-latitudes (Hösen et al., 2014). The vortex index provides an altitude-independent information whether a measured air mass originally came from the interior of the vortex of from outside. Therefore the COPAS measurements can be categorized with respect to their recent origin by means of the index ξ_{vi} rather than considering only their actual position inside or outside the vortex. For altitudes with potential temperature Θ above 400 K, ξ_{vi} implicitly provides a measure for the mixing of inner vortex air with air from outside. The higher the values of ξ_{vi} are, the more pristine, undiluted inner vortex air was probed. The criteria defined for this study to classify the COPAS measurements for Θ levels above 400 K are:

1. $\xi_{vi} > 0.75$: sample air originating mostly from the vortex interior, with admixed mid-latitude incorporations of less than 25 %.

2. $0.75 < \xi_{vi} < 0.25$: sample air with extra-vortex mid-latitude air contributions which are too large for unambiguous apportioning.

ACPD
14, 9849–9901, 2014

3. $\xi_{vi} < 0.25$: sample air originating from well outside of the polar vortex, mostly consisting of mid-latitude air.

The COPAS measurements are recorded with 1 Hz temporal resolution. One single N_2O data point is measured by HAGAR (representative for air sampled during 2–3 s) only once every 90 s, which then also is the temporal resolution of the vortex index ξ_{vi}. Each ξ_{vi} value is associated with five COPAS readings, extending from two seconds before the HAGAR measurement point to two seconds after. This way also a possible discrepancy between the controller time set of COPAS and HAGAR ($\sim$ 1 s) is compensated. Those COPAS measurements which are not attributable to a value of N_2O mixing ratio or vortex index are excluded from the analysis. The results of the COPAS measurements from EUPLEX (2003) were already discussed in detail by Curtius et al., 2005. However, these analyses apportioned the data records to the vortex interior or exterior by means of the chemistry transport model CLaMS (McKenna et al., 2002a, b; Konopka et al., 2007; Grooß et al., 2014; see also below). The results from 2003 discussed here are re-calculated adopting the empirical measure of ξ_{vi} based on in situ observations during EUPLEX. Consequently the analysis of EUPLEX data here is based on a different approach, though the conclusions from this re-calculation do not differ from the interpretation of Curtius et al., 2005. A detailed discussion regarding the correspondence between the empirical ξvi, based on N_2O measurements, and the air origin assignment by means of inert artificial tracers in the ClaMS model (cf. below) is provided in Hösen et al., 2014.

2.3 Meteorological measurements

Ambient air temperature and static pressure were measured with the Thermo Dynamic Complex (TDC) probe with 1 Hz resolution and an accuracy of 0.5 K (Shur et al., 2007). If TDC data were not available (e.g. throughout ESSenCe) temperature and pressure data were adopted from the Unit for Connection with the Scientific Equipment (UCSE, Sokolov and Lepuchov, 1998), a part of the navigational system of the M-55

ACPD
14, 9849–9901, 2014

Geophysica providing 1 Hz-resolved ambient pressure (with accuracy of ±1 hPa) and temperature (±2 K accuracy) data.

2.4 CLaMS modelling

Model simulations with the 3-dimensional Chemistry Transport Model (CLaMS) (McKenna et al., 2002a, b; Konopka et al., 2007; Grooß et al., 2014) were performed with extensive stratospheric chemistry, including heterogeneous chemistry and particle sedimentation, driven by ERA-Interim reanalysis data for the EUPLEX, RECONCILE and ESSenCe campaigns. For all simulations a suite of inert artificial tracers was utilized, which mark particular regions in the atmosphere (e.g. vortex air and mid-latitude air, according to the Nash-criterion) at the beginning of each simulation. The advection and mixing of the marked air parcels is then modelled by the CLaMS transport scheme, which allows the tracking of the air mass and the detection of its origin (Günther et al., 2008) covering the Northern Hemisphere. For EUPLEX and RECONCILE the CLaMS simulations were conducted with a horizontal resolution of approximately 70 km and a maximum vertical resolution of about 400 m around the tropopause. The simulations were initialized at the beginning of the winter, usually at 1 December, using satellite measurements and tracer-tracer correlations following Grooß et al., 2014. For ESSenCe the CLaMS simulations were initialized on 1 November 2011 and yielded a horizontal resolution of 100 km. For our study, an analysis of the tracer distributions lead to the determination of the horizontal vortex cross section area (VCSA) averaged for respective campaign within the altitude range covered by the in situ measurements, i.e. between 400 and 500 K of potential temperature. For this altitude range the VCSA is obtained by means of CLaMS model calculations in altitude steps of 10 K of potential temperature as a mean value of each Θ-step ± 5 K. The calculated VCSAs exclude any air recently intruded from mid-latitudes for which the selected observations would not be representative.

ACPD
14, 9849–9901, 2014

2.5 Total mass of refractory aerosol matter

The total refractory aerosol mass within the observationally covered altitude range (400 K < Θ < 500 K) inside the vortex is estimated in principle by (a) subdividing the vortex column into 10 vertical layers, each of ΔΘ = 10 K thickness, (b) calculating the total mass of the refractory aerosol from the measured N_{10}nv (as function of Θ) inside each VCSA-disk assuming certain particle number size distributions which are converted into volume/mass distributions, and (c) adding up the aerosol masses of all vertical layers. In more detail, our estimates are based on parameterizations of the in situ measurements (cf. Sect. 5) and on the following assumptions:

1. inside the vortex, the mixing ratio of refractory aerosols, parameterized as a function of Θ, is assumed to be constant across the surface of each VCSA level. Furthermore, the values are assumed to be time-invariant during the relatively short campaign periods of 3–4 weeks resembling a snap-shot picture of the downwelling motion inside the vortex.

2. The size distribution of the refractory aerosol material is assumed to be constant and within the range of size distributions provided by three different studies: Jaenicke, 1980; Wang et al., 1989, and Deshler, 2008 (cf. Fig. 1). The integrals over the resulting model size distributions are scaled such that they represent the absolute values of the refractory aerosol total mixing ratios.

3. The particle material density ρ_p is estimated to be at about 1400 kg m^{-3}, with an uncertainty ranging from 1000 to 2000 kg m^{-3}. Though in former studies a value of ρ_p of 2000 kg m^{-3} was used – referring to the density of a typical stone meteorite (Chondrite, e.g. Hunten et al., 1980 or Plane, 2004) – we use ρ_p of 2000 kg m^{-3} as the upper limit. This implies that vaporized meteorites and ablation smoke recombine to a somewhat porous material instead of solid particles, having an effective density lower than the original material.

ACPD
14, 9849–9901, 2014

4. For estimating the particle burden as function of model pressure altitude, a relation between the potential temperature Θ (in K) and the atmospheric pressure p (in hPa) is needed, which is derived from parameterizations of the measured Θ-p-relationship.

This way the total mass of refractory aerosol contained inside the polar vortices of each campaign can be coarsely estimated and compared to the total mass influx of meteoric material entering the atmosphere.

3 Field campaigns in the years 2003, 2010 and 2011

Three measurement campaigns were carried out in the Arctic winter seasons of the years 2003, 2010 and 2011, from Kiruna, Northern Sweden (67°49′ N, 20°30′ E) deploying the high altitude research aircraft M-55 *Geophysica* (Stefanutti et al., 1999), which is capable of operating at altitudes of up to 20 km:

1. EUPLEX, January–March 2003: 15 mission flights
   - EUropean Polar stratospheric cloud and Lee wave EXperiment (Günther et al., 2008)
   - combined with the European space agency (ESA) ENVISAT – Arctic Validation Campaign,
2. RECONCILE, January–March 2010: 13 mission flights
   - Reconciliation of essential process parameters for an enhanced predictability of Arctic stratospheric ozone loss and its climate interactions (von Hobe et al., 2013).
   - completed by a two-flight mission PremierEX (Spang et al., 2012) and
3. ESSenCe (ESa Sounder Campaign), December 2011: 2 mission flights (Kaufmann et al., 2014).

ACPD
14, 9849–9901, 2014

The flight activities during EUPLEX/ENVISAT-validation (in the following denoted as EUPLEX) took place between 10 January through 19 March 2003 with a downtime between 11 and 28 February. Stratospheric air mass exchange between the interior and exterior of the polar vortex during EUPLEX was analyzed by Günther et al., 2008, and further discussed by Werner et al. (2010). In summary, during the EUPLEX period, two major vortex break-up events happened: (a) from 21 January through 23 January, and (b) between 15 February until 23 February. Both were followed by vortex recombination (Günther et al., 2008).

RECONCILE/PremierEX (abbreviated as RECONCILE) was conducted between 17 January and 10 March 2010. During RECONCILE, there was a downtime between 2 and 27 February (cf. von Hobe et al., 2013). As described by Dörnbrack et al., 2012, the polar vortex disintegrated into two parts around 15 December 2009, just prior to the RECONCILE flight operations, and recombined around 25 December 2009. A second vortex break-up occurred in mid-February, followed by recombination in early March. During both break-up events the coldest of the two vortex fragments survived and regenerated. The regeneration period to recover a compact vortex structure lasted until beginning of January 2010 and beginning of March 2010, respectively. The simulation of inert artificial tracers in the CLaMS model indicates that the first vortex split in December 2009 caused a strong exchange and dilution of air inside the vortex with air from lower latitudes. In contrast, the second vortex split negligibly influenced the air composition inside the vortex during the second campaign period. After regeneration, at the beginning of March 2010, the air chemical composition inside the vortex was rather homogenized compared to conditions following the first vortex split in December 2009.

Both missions, EUPLEX and RECONCILE, covered the same seasonal time in the Arctic winter and early spring period. For EUPLEX and RECONCILE the data of the first and second phases before and after the downtimes are denoted with suffixes -A and -B.

ACPD
14, 9849–9901, 2014

ESSenCe was performed during December of 2011, i.e. early in the winter season, although in this particular year the vortex had already developed. In contrast to the more disturbed and warm Arctic winters 2002/03 and 2009/10, the vortex during ESSenCe remained mainly unperturbed, resulting in the formation of a strong horizontal transport barrier and very cold temperatures (below 192 K at the 50 hPa pressure level) already in December 2011. During the ESSenCe winter extended fields of persisting synoptic scale PSCs were observed and probed (Molleker et al., 2014; Woiwode et al., 2014).

4 Observations and results

4.1 Particle abundances inside and outside the vortex

The measured aerosol mixing ratios in the Arctic winter stratosphere are summarized in Fig. 2 through Fig. 4. For Θ above 400 K and for ξ_{vi} below 0.25, i.e. outside the polar vortex, the mixing ratio N_{10} remains fairly constant at about 150 to 300 mg^{-1} and slightly decreases with increasing Θ above 440 K to values below 200 mg^{-1} (Fig. 2). For variable mixing states of vortex air with mid-latitude air (i.e. $0.25 < \xi_{vi} < 0.75$), N_{10} never exceeds 300 mg^{-1}, but is usually constrained to lower values between 100 and 200 mg^{-1}. In contrast, N_{10} continuously increases with Θ in the vortex ($\xi_{vi} > 0.75$). This is particularly obvious in Fig. 2a from the vertical profile of N_{10} for the EUPLEX-A period. Also, during EUPLEX-A the mixing ratio of non-volatile particles follows the same behavior as function of altitude (Fig. 2b).

Inside the polar vortex N_{10}nv increases considerably with rising Θ, and significantly exceeds the magnitude of N_{10}nv outside vortex. The fraction f of non-volatile particles (Fig. 2c) for EUPLEX-A outside of the vortex generally remains below 50 % (ranging mainly between 10–35 % for $\Theta > 400$ K). Variable mixing stages of the vortex air (i.e. $0.25 < \xi_{vi} < 0.75$) go along with values for f between 25–60 %. Inside the polar vortex f is generally larger than 50 % and reaches up to 80 % during EUPLEX-A. During

ACPD
14, 9849–9901, 2014

EUPLEX-B (Fig. 2d) in principle the vertical dependence of N_{10} is similar to EUPLEX-A. However, despite the fact that the M-55 *Geophysica* operated at its maximum ceiling, the high Θ levels of EUPLEX A inside and outside the vortex could not be reached during EUPLEX B. Nevertheless, N_{10}nv from Fig. 2e resembles the observations of EUPLEX-A. While differences in f between inside and outside the vortex are visible in both data sets, the highest values of up to 80 % were measured during EUPLEX-A.

The vertical profiles of the aerosol mixing ratio from RECONCILE are similar in shape to those from EUPLEX. During RECONCILE-A N_{10} does not significantly differ between inside and outside the vortex (Fig. 3a). The vertical profile of N_{10}nv (Fig. 3b) indicates that the mixing ratio of refractory aerosol increases inside the vortex where also highest values of the fraction f (Fig. 3c) are reached. During RECONCILE-A the inside and outside vortex distributions are clearly less distinct, compared to EUPLEX. This lack of contrast could be due to significant dilution of the vortex content with mid-latitude air associated with the vortex break-up and recombination prior to RECONCILE-A. In RECONCILE-B, mainly measurements outside the polar vortex were performed with the highest levels of potential temperature above 510 K. Here N_{10} (Fig. 3d) shows a nearly constant profile with values at about 100 mg^{-1} for Θ larger than 400 K. Only few measurements could be performed well inside the polar vortex during RECONCILE-B. These show in contrast to RECONCILE-A a considerable increase in N_{10} from about 80 to nearly 180 mg^{-1} as function of Θ between 400 and 460 K.

Particle mixing ratios measured during ESSenCe, in December 2011, are generally lower compared to EUPLEX and RECONCILE (Fig. 4a) with values of N_{10} smaller than 100 mg^{-1} for Θ above 400 K. However, the shape of the vertical profile of N_{10}nv (Fig. 4b), exhibits a steeper increase with altitude than N_{10}, which agrees qualitatively with corresponding results of the previous campaigns. As a consequence, similarly high values of f are found (Fig. 4c). This means that also during ESSenCe, the highest fractions of f were observed inside the polar vortex reaching values between 60 and 80 %.

ACPD
14, 9849–9901, 2014

During all three missions recent new particle formation did not occur inside the probed air sectors and, therefore, ultrafine particles with diameters smaller than 10 nm did not detectably contribute to the measured particle mixing ratios.

All observed vertical profiles for the submicron particle mixing ratios are comprehended into Fig. 5 in terms of medians with percentiles:

4.1.1 Outside the polar vortex

For Θ levels above 400 K, the vertical distribution of N_{10} shows the lowest values for all altitudes in the earliest winter period (ESSenCe, Fig. 5a). Later in the winter the total mixing ratios are higher by a factor of 1.2 to 2.5: N_{10} either remains constant with altitude (RECONCILE, Fig. 5i) or is rather variable (i.e. reaching an enhancement by a factor of up to 2.5 during EUPLEX, Fig. 5e). During EUPLEX, a considerable difference in the vertical distribution of N_{10} exists between the A- and B- periods, which might be related to an air mass exchange with mid-latitudes during the vortex break-up (Curtius et al., 2005; Werner et al., 2010). The mixing ratios of refractory particles are similar with about 30 to 50 mg^{-1} for all late-winter situations (Fig. 5f and j). In contrast the values are between 20 and 35 mg^{-1} and thus lower during early winter (Fig. 5b). This results in similar fractions f of 25 to 50 % for ESSenCe (Fig. 5d) and EUPLEX (Fig. 5h). The entry of mid-latitude air masses into the Arctic lower stratosphere just prior to the EUPLEX-B period might be indicated by the decreased f (Fig. 5h, open red circles) for Θ levels higher than 420 K. At the same time the mixing ratio difference $N_{10} - N_{10}$nv increases for the EUPLEX-B period in the same altitude range (Fig. 5g) which supports the impression that air was isentropically exchanged. During RECONCILE (Fig. 5l), the fraction f is generally higher, attaining 30 %, and 50 % for Θ below 450 K. Further aloft (450 K < Θ < 510 K) f is increasing up to 60 % outside the polar vortex. However, these high Θ levels were only reached outside the vortex during the second winter period of the year 2010 (RECONCILE-B) and comparable data are not available from the other campaigns.

ACPD
14, 9849–9901, 2014

4.1.2 Inside the polar vortex

For Θ levels exceeding 400 K, the increase of N_{10} and N_{10}nv with Θ is considerably steeper than outside the vortex. Additionally the gradient of the enhancement of N_{10}nv with Θ is stronger than for N_{10}. Differences between the A- and B- phases of EUPLEX and RECONCILE result mainly from the air mass descent within the vortex. Although N_{10} is comparably low during ESSenCe (Fig. 5a), the increase of N_{10}nv with Θ (Fig. 5b) is steeper than that of N_{10}. The resulting fractions f (Fig. 5d) coincide well with the corresponding values obtained from EUPLEX and RECONCILE (Fig. 5h and l) in the same Θ range. This is particularly the case when compared with corresponding values from EUPLEX-A and RECONCILE-B. The decreased values of f for EUPLEX-B compared to EUPLEX-A cannot be explained by descent within the vortex and are likely due to the large-scale dilution of the vortex in March 2003 (Günther et al., 2008). Apparently the details of the polar winter vortex meteorology leave discernible imprints in the vertical aerosol particle distribution.

The strongest increases of f with Θ were observed inside the vortex during EUPLEX-A, RECONCILE-B – with less disturbed vortex conditions for a certain period prior to the observations – and during ESSenCe when the vortex had just recently developed. Fractions f of non-volatile particles as high as 70 % were found in the vortices at potential temperatures of 450 K. Only for EUPLEX-A and RECONCILE-B the median values for f exceed 70 % at higher altitudes (e.g. at about 470 K in RECONCILE-B, Fig. 5l). Considering the 75-percentile also f values can be observed which are even higher than 75 % at Θ level 480 K (EUPLEX-A, Fig. 5h). In the Θ range above 480 K only data from EUPLEX-A indicate a slight decrease of f with increasing potential temperature.

4.1.3 The contribution of volatile particles

The contribution of volatile particles is accounted for with the mixing ratio difference given as $N_{10} - N_{10}$nv. However, also partly-volatile particles may be included in this value (i.e. refractory residuals smaller than 10 nm which are not detected with the N_{10}nv

ACPD
14, 9849–9901, 2014

COPAS channel, coated with volatile substances resulting in a particle size larger than 10 nm which the N_{10} detector is sensitive for). The mixing ratio difference during ESSenCe (Fig. 5c) decreases for Θ above 400 K outside the vortex and remains nearly constant as function of altitude inside the vortex. For EUPLEX (Fig. 5g) $N_{10} - N_{10}$nv increases inside the vortex much less steeply with altitude than N_{10}nv. Surprisingly, for the RECONCILE case (Fig. 5k) very similar values of $N_{10} - N_{10}$nv with Θ are measured inside and outside of the vortex as well as during RECONCILE-A and RECONCILE-B. Most likely the reason behind is inherent in the vortex instability. During RECONCILE the vortex was more disturbed and inhomogeneous than during EUPLEX or ESSenCe (cf. Sect. 3).

In summary, increasing particle mixing ratios inside the Arctic vortex are mainly due to increasing refractory aerosols with altitude. The fact that N_{10}nv and $N_{10} - N_{10}$nv behave differently indicates that N_{10}nv has sources that are decoupled from those of the mainly volatile portion of the detected aerosol. Essentially the constant values of $N_{10} - N_{10}$nv observed inside and outside the vortex over the complete RECONCILE mission period may be a result of exceptionally warm stratospheric temperatures. However, for the RECONCILE case this means: (a) increasing particle mixing ratios as function of altitude inside the vortex are solely supplied by non-volatile particles as otherwise $N_{10} - N_{10}$nv would show a similar increase with altitude, and (b) if $N_{10} - N_{10}$nv includes small non-volatile residuals ($d_p < 10$ nm), then the particles subsiding in the vortex during RECONCILE predominantly consisted of non-volatile particles larger than 10 nm.

4.2 Particle mixing ratio as function of N_2O mixing ratio

In Fig. 6 the particle mixing ratios N_{10}nv and the fractions f are correlated with the concurrently in situ measured abundances of the long lived tracer N_2O. Since the N_2O mixing ratios monotonously decrease with rising altitude in the stratosphere, the ordinates in Fig. 6 are reversed.

ACPD
14, 9849–9901, 2014

For all three missions increasing mixing ratios of non-volatile particles coincide with decreasing N_2O mixing ratio, as also do the enhanced relative contributions to the total aerosol abundance. This seems to be closely linked to the downward transport of air masses from higher altitudes inside the vortex. For near-tropospheric N_2O mixing ratios ($< 300\,\mathrm{nmol\,mol^{-1}}$) positive correlations, i.e. reductions of N_{10}nv and f with decreasing N_2O mixing ratio, are found. At lower N_2O mixing ratios (or higher altitudes in the lower stratosphere), there is no or just a slight anti-correlation, i.e. increasing N_{10}nv and f with decreasing N_2O mixing ratios. At values for N_2O below $200\,\mathrm{nmol\,mol^{-1}}$ – typical values in the Arctic lower stratosphere – a clear anti-correlation is observed showing rising N_{10}nv and f with decreasing N_2O. These low N_2O values (down to $70\,\mathrm{nmol\,mol^{-1}}$) indicate that air masses were transported downward from higher altitudes in the stratosphere. The higher concentrations of refractory particles thus are an indication of such non-volatile materials being supplied from above. As this anti-correlation is very similar for the late-winter campaigns of EUPLEX and RECONCILE, it is apparently not a unique event. For ESSenCe, unfortunately no flights were conducted in the late winter season.

The mixing ratio N_{10}nv generally increases faster than N_{10} with decreasing N_2O inside the vortex. As a consequence, the fraction f of non-volatile particles grows with altitude and falling N_2O, and refractory aerosol particles increasingly contribute to the enhanced particle mixing ratios. The ratio f is shown in Fig. 6f through Fig. 6j as a function of the N_2O mixing ratio. For N_2O mixing ratios below $175\,\mathrm{nmol\,mol^{-1}}$, the fraction of non-volatile aerosol ranges at about 50 %, or higher, and increases further aloft to values of up to 80 % (EUPLEX-A – Fig. 6g, RECONCILE-B – Fig. 6j or ESSenCe – Fig. 6f). Contrary to N_{10}nv the gradients of the fraction f with decreasing N_2O seem to compare well throughout all cases. This includes the measurements from ESSenCe as well and appears to be independent of the progress of the respective winter season.

In summary, the observations reveal that inside the polar vortex and at potential temperature altitudes between 490 and 500 K up to 150 particles per milligram from total mixing ratios near $200\,\mathrm{mg^{-1}}$ (N_{10}) were identified to be thermally stable at 250 °C. This

ACPD
14, 9849–9901, 2014

means a very large fraction of up to 8 of 11 particles per cm^3 (at ambient conditions) contain materials which are not sulfuric acid, water, nitric acid or others which evaporate at temperatures below 250 °C. For these reasons a strong presence of meteoric ablation materials can be assumed although detailed chemical analyses of such particles in the submicron size range still are scarce.

5 Discussion

5.1 Vertical profiles of non-volatile particle mixing ratio

Air masses originally coming from the upper stratosphere subside over the course of the winter within the Arctic polar vortex as indicated at a given altitude by N_2O mixing ratios substantially decreasing with time. This is also verified and quantified by numerical studies (Prather and Rodriguez, 1988; Fisher et al., 1993; Plumb et al., 2002). Remarkably enhanced mixing ratios of carbon monoxide and molecular hydrogen coinciding with low values of SF_6 (Engel et al., 2006) show particularly strong downwelling of air even from the mesospheric levels during the 2003 EUPLEX winter (January through March).

The study of Wilson et al., 1990, already described increasing submicron aerosol concentrations with altitude inside the Arctic vortex by measurements utilizing the NASA *ER-2* aircraft during the Airborne Arctic Stratospheric Expedition (AASE) in January and February 1989. Further evidence for an increasing number concentration of so-called condensation nuclei (CN; in the older nomenclature particles detectable by a condensation particle counter) was found from balloon-borne measurements at Kiruna in January of the year 1990 (Hofmann et al., 1990, Fig. 1a therein). However, Wilson et al., 1990, suggested that homogeneous nucleation of the H_2SO_4/H_2O system might have been the source of these particles in the Arctic winter stratosphere. Recent new particle formation was never observed throughout our Arctic measurements, as increased concentrations of ultrafine particles (with 6 nm < d_p < 15 nm) were

ACPD
14, 9849–9901, 2014

not detected. In addition, the particle mixing ratio difference $N_{10} - N_{10}$nv (Fig. 5) remains fairly constant inside and outside the vortex with altitude (ESSenCe, Fig. 5c, RECONCILE Fig. 5k). Or, when it does increase with altitude, N_{10}nv increases more strongly (EUPLEX, Fig. 5f and g) particularly inside the vortex. Thus, it seems apparent that increasing particle mixing ratios with altitude are mainly linked to a supply of refractory particles from higher altitudes. However, it cannot be ruled out that further refractory residuals were too small ($d_p < 10$ nm) to be detected with COPAS. It is possible that the observations made by Wilson et al., 1990, also included a major fraction of refractory aerosol material imported from aloft. Under this assumption, and considering the observations by Curtius et al., 2005, from the EUPLEX (2003) winter together with our findings of this study, we hypothesize that this particle import is a regular feature of the late winter polar vortex in the Northern Hemisphere, provided that it develops throughout the season sufficiently undisturbed from mid-latitude in-mixing.

5.2 Correlations of non-volatile particles with tracer N_2O

As shown in Fig. 6a through Fig. 6e the enhancement of refractory aerosol particles larger than 10 nm with decreasing N_2O inside the vortex results in a rather compact (anti-)correlation of N_{10}nv and N_2O as indicated by the linear fits for data points with ξ_{vi} higher than 0.75. The slope of this correlation is much smaller for the ESSenCe period in December 2011 (Fig. 6a) than for the other cases, and the highest slopes are found for the EUPLEX-B and RECONCILE-B periods in late winter.

The observed correlations between the long-lived tracers N_{10}nv and N_2O can be consistently interpreted in terms of the theory of stratospheric tracer-tracer correlations, which is well developed and verified (cf. Plumb, 2007, and references therein) by observations. In the absence of the polar vortex, rapid isentropic mixing creates a unique extra-tropical canonical relation between two long-lived tracers, the shape of which is determined by the vertical distribution of the respective sources and sinks. In particular this canonical correlation is expected to exhibit curvature in the region close to sinks or sources of either compound, but to be linear elsewhere. After the formation

ACPD
14, 9849–9901, 2014

and ensuing subsidence of the polar vortex, the polar transport barrier isolates vortex air with the consequence that the correlation within the vortex may change over the course of the winter resulting in a vortex correlation distinct from the original canonical correlation. In the present case, the observed positive correlation and curvature at the highest N_2O, above 200 nmol mol^{-1}, is indicative of a lower stratospheric sink of particles with tropospheric origin, presumably due to particle growth and gravitational settling, and strat-trop exchange events. This canonical correlation could not be observed for N_2O values below 200 nmol mol^{-1}, which at mid-latitudes (ξ_{vi} values below 0.25) generally occur only above 20 km. Instead, its expected shape is illustrated qualitatively in Fig. 6 (range between the grey lines in Fig. 6a to e) based on the observations within the vortex (red data points) and the following considerations:

1. for N_2O smaller than 200 nmol mol^{-1}, the canonical correlation is expected to proceed approximately linear with a slope determined by the mid-stratospheric N_2O sink and a particle source at higher altitudes (presumably in the mesosphere).

2. When the sink of N_2O becomes efficient (at $N_2O < 70$ nmol mol^{-1}), the canonical correlation will curve toward higher particle mixing ratios (e.g. steeping slope of canonical correlation indicated with gray lines in Fig. 6a) until all N_2O has been lost, at which point it continues (outside the displayed range) horizontally as refractory aerosols still increase due to the mesospheric source. This canonical correlation is expected to be present also at high latitudes until the fall and possibly early winter. (Hence it may actually be similar to the ESSenCe observations during December; cf. Fig. 6a.)

3. However, as the winter proceeds the descent and dynamical isolation of the vortex (with N_2O values below about 200 nmol mol^{-1}) progressively leads to a vortex correlation that separates toward the concave side of the curved canonical correlation (progressing distance of data points from the canonical correlation, towards higher particle mixing ratios in Fig. 6b to e). This generally results in less curved,

ACPD
14, 9849–9901, 2014

or over some range approximately linear correlations, inside the vortex just as actually observed here.

4. The deviation may still be negligible early in the winter (ESSenCE, Fig. 6a), but increasingly pronounced in mid and late winter resulting in steeper slopes (EUPLEX: Fig. 6d or RECONCILE: Fig. 6f). For N_2O values smaller than $50\,\mathrm{nmol\,mol^{-1}}$, which is beyond the sink region of N_2O, and outside the range displayed in Fig. 6, the vortex and the canonical correlation will eventually re-converge until they become identical, namely horizontal, in the upper stratosphere when N_2O mixing ratios reach zero.

In order to evaluate similarities and differences of the gradient as function of Θ and the N_2O mixing ratio Fig. 7 shows the corresponding scatter plots. Note that only measurement points from the vortex interior are displayed and that the scale of the color code extends from 0.75 to 1.0 for ξ_{vi}. The plots exhibit roughly linear relationships over most of the observed range. From the RECONCILE data set shown in Fig. 7b and e, nevertheless, it can be seen that the functions $N_{10}nv(\Theta)$ and $N_{10}nv(N_2O)$ are not linear over the entire range of Θ and N_2O. Instead, there is a much smoother increase for $380\,K < \Theta \leq 410\,K$ compared to $\Theta > 410\,K$. The data points of the altitude range below 410 K are shown as crosses instead of circles (Fig. 7b), similarly for the EUPLEX (Fig. 7a) and ESSenCe (Fig. 7c) data. The deviation from a single straight line is most pronounced for RECONCILE. For ESSenCe, there might not have been enough data points or, more likely, the distinct gradients for altitudes above 410 K had not yet developed during early winter. The two different correlations of the two altitude bands may arise from the dynamics at the vortex bottom. Below 410 K (Fig. 7b), the vortex boundary does not act anymore as an effective transport barrier thus allowing for more efficient isentropic exchange and mixing with the mid-latitudes (Haynes and Shuckburgh, 2000). As a result, in this region no separate vortex correlation forms; instead the canonical curve is observed at all (extra-tropical) latitudes. Observational indications for the existence of such a transition zone were indeed already described

ACPD
14, 9849–9901, 2014

by Weinheimer et al., 1993. Borrmann et al., 1995, identified this transition zone below the vortex bottom also by linear correlations between aerosol (surface area) mixing ratio and a tracer (there ozone; here N_2O) for a very similar potential temperature altitude range. The described discontinuity is not only present in the linear correlations between the mixing ratio N_{10}nv and potential temperature but also in those between N_{10}nv and N_2O for RECONCILE (Fig. 7e). This clearly shows that different air masses are involved, and we presume that increased isentropic mixing in connection with efficient air mass exchange at the vortex bottom outflow region causes the observed discontinuity. A similar, although much less pronounced discontinuity is also observed for ESSenCe, while for EUPLEX there are too few observations at the vortex bottom to discern it.

All linear regressions of N_{10}nv vs. potential temperature and N_2O mixing ratios from the three field campaigns are shown in Fig. 8, together with the 95 %-confidence intervals and with the resulting regression parameters provided in Table 1. The regressions were performed separately: once for measurement points associated with potential temperatures below and once for those above 410 K. The lines from the different campaign years in Fig. 8a which show the correlations with potential temperature, significantly differ from each other. Obviously the dependency of N_{10}nv on Θ strongly depends on the large-scale dynamics of the vortex, in particular on the strength of vortex descent and on the vortex stability over the winter period. The observed vertical gradients of the three campaigns are qualitatively consistent with continuing diabatic descent of vortex air (and thus surfaces of N_{10}nv), which due to the increase in density is expected to steepen the gradients over the course of the winter. Thus the smallest vertical gradient is observed for ESSenCE (December) and the largest for RECONCILE, where the regression is dominated by the March observations up to 470 K. The corresponding values for EUPLEX lie in between. Here the regression is dominated by the January data up to 500 K. Notably, the regressions of N_{10}nv for the bottom vortex region have similar slopes and only differ in the absolute numbers between RECONCILE and ESSenCe. Because of the lack of an efficient transport barrier and weak descent

ACPD
14, 9849–9901, 2014

at these lower altitudes the vertical gradient in the transition region is apparently less dependent on the dynamical state of the vortex.

In terms of the correlation between N_{10}nv and N_2O (Fig. 8b) the agreement of the regression slopes between EUPLEX (i.e. -0.71 ± 0.05) and RECONCILE (i.e. -0.68 ± 0.01) is remarkable. Only the absolute values of N_{10}nv are shifted along the ordinate by a factor of about 1.1. Note that in terms of the covered range of N_2O mixing ratio, measurements of RECONCILE-B dominate the regression compared to the RECONCILE-A period (cf. Fig. 6a–e together with Fig. 7d through Fig. 7f), and the data from the later mission period assume more weight in the regression calculation. Such a weighting imbalance is less pronounced for the EUPLEX period although the lowest N_2O mixing ratios were detected predominantly during the earlier EUPLEX period. Finally, the slopes and intercepts of the ESSenCe data regressions are quite different from those of the other missions. The observed correlations are qualitatively consistent with the expected development of the N_{10}nv-N_2O correlation inside the vortex over the course of the winter (as outlined above). Starting from the original canonical mid-latitude correlation at the time the vortex forms, vertical dispersion inside the isolated vortex will continuously act to increase N_{10}nv on a given N_2O surface, consistent with the observed increase between ESSenCE (December), EUPLEX (more weighted toward January data) and RECONCILE (dominated by March data). Considering the results of all of three winters we thus conclude that in addition to diabatic descent, efficient downward transport of refractory particles from the upper stratosphere and mesosphere is achieved by vertical dispersion (resulting from differential subsidence together with horizontal stirring) inside the vortex, in accord with current understanding of polar tracer transport (Plumb et al., 2002 and Plumb, 2007).

5.3 Implications for PSC formation

The import of refractory aerosol material by subsidence and vertical dispersion within the vortex constitutes a strong source of particles for a region where the relative isolation of the vortex supports chemical reactions. The non-volatile particles carried from

ACPD
14, 9849–9901, 2014

aloft are most likely incorporated by stratospheric sulfate aerosol or covered with sulfuric acid and provide surfaces for condensable materials and heterogeneous chemical reactions (Peter, 1997; Wegner et al., 2012). PSC formation is usually thought to occur by heterogeneous nucleation on the homogeneously nucleated H_2SO_4-H_2O-droplets of the stratospheric background aerosol. It may be hypothesized that stratospheric cloud elements also and possibly even preferably form on pre-existing condensation surfaces (Hoyle et al., 2013; Engel et al., 2013) as provided by refractory particles, eminently in times when stratospheric background aerosol concentrations are low. In particular this process may be relevant in a weakly HNO_3-supersaturated polar stratosphere (Voigt et al., 2005), which is a frequently occurring condition in the Arctic. Nevertheless, based on our data it cannot be excluded that a certain fraction of stratospheric cloud particles may form via new particle formation at even higher altitudes than explored by our mission flights, although above some altitude the temperatures will become too large and the sulfuric acid vapor concentrations too low for this.

5.4 Estimates of the refractory aerosol mass in the vortex

In this section we estimate the total amount of refractory submicron aerosol contained inside the Arctic vortex during our observation periods of the winters of 2003, 2010 and 2011 in the altitude range covered by the measurement flights.

For the estimation the following steps were applied:

1. the vortex cross sectional areas (VCSA) are calculated by means of the CLaMS model in potential temperature bins of 10 K for Θ between 400 and 500 K averaged over the respective campaign duration (cf. Sect. 2) with the results shown in Table 3. The determined VCSAs include the (horizontally) rather homogeneous parts of the vortex for which the selected observations with values of ξ_{vi} higher than 0.75 are representative. Thus, air recently intruded from mid-latitudes is not included this way.

ACPD
14, 9849–9901, 2014

2. Based on the regressions shown in Fig. 8a, the mixing ratios N_{10}nv are parameterized as a function of the potential temperature (Table 1).

3. A range of mean particle volumes based on the range of stratospheric aerosol size distributions (cf. Sect. 2 and Fig. 1) is calculated.

4. Particle volume ratios per air mass ($m^3\,kg^{-1}$) are calculated from N_{10}nv and the size distributions from Step (3) as a function of the potential temperature.

5. A range of the Θ-p-relationship is parameterized based on measurements for the respective Arctic campaign and its variability (Table 2) because for the necessary air volume/mass calculations the ambient pressures and temperatures are needed. Total particle volumes and total particles masses (under consideration of a range of densities for the particulate material, cf. Table 2) are calculated for each potential temperature bin from the particle number densities.

6. From this set of data the total particle volume and the total particle mass are calculated as well as the mass of the air the particles are contained within. The masses are summed over all potential temperature bins between 400 and 500 K (Table 3), where particle data were available.

Of course there are uncertainties inherent in such estimates:

(a) about a factor of 20 in uncertainty arises from the unknown true size distribution of particles with diameters between 10 nm and 3 µm, because COPAS detected the particles but did not size them.

(b) Further uncertainties of a factor of two come from the Θ-p-relationship, and an additional factor of two from the particles material density ρ_p.

(c) Also it has to be considered that substantial amounts of refractory aerosol vertically transported by the vortex from above are not accounted for in our approach. Examples are particles in the vortex edge region or within and below the vortex

ACPD
14, 9849–9901, 2014

bottom transition zone, and particles horizontally transported from the vortex to mid-latitudes prior to the observation period.

(d) Due to the COPAS activation limit and the inlet transmission, particles of diameters smaller than 10 nm and larger than few µm are disregarded. However, extrapolating from the literature size distributions, the contribution of these size ranges to the background aerosol mass is expected to be minor.

(e) The model estimates of VCSA involve uncertainties of at most 50 % as well.

In Table 3 the results of our estimates are provided in terms of the altitude resolved mass of refractory aerosol and as a function of the potential temperature. The applied pressure altitudes for the respective Θ levels indicate the various meteorological vortex conditions of the different campaigns. The resulting estimate amounts to a mass of approximately 32×10^6 kg of refractory aerosol in the vortex column between 85 and 49 hPa for EUPLEX. The ESSenCe case with estimated 13×10^6 kg of refractory particulate matter between 101 and 56 hPa may provide a reference for the conditions when the vortex air is not yet influenced by major particle import from aloft during the current winter. The largest estimated mass in the probed vortex column comes from the RECONCILE measurements. These are dominated by data from March, i.e. the late Arctic winter, and the calculated total refractory aerosol mass is about 53×10^6 kg in the pressure range between 131 and 67 hPa.

Within a pressure range from 100 to 67 hPa the derived refractory aerosol masses from RECONCILE (39×10^6 kg) and ESSenCe (7×10^6 kg) are directly comparable. Presuming the vortices to undergo similar developments throughout the different winters (which is not necessarily the case), the mass difference constitutes an enhancement on the order of 32×10^6 kg (a factor of 5.5) of refractory aerosol over three months from December through March. This constitutes a considerable abundance of refractory aerosol material inside the lower vortex regime with conceivable significance for PSC formation. Despite the coarseness of such estimations the resulting masses may

ACPD
14, 9849–9901, 2014

represent literally only the tip of the iceberg, because the vortex volume above the pressure-altitude of 67 hPa is not accounted for with our approach.

According to model studies of vertical vortex transport (e.g. Plumb et al., 2002) towards the end of a polar winter the content of the whole mesosphere is ingested by the vortex and the signatures of air of mesospheric origin are discernible down to lower regions within the vortex. Previous balloon-borne observations of carbon monoxide (CO) have traced mesospheric origin up to levels higher than 500 K of potential temperature (see Fig. 6 in Plumb et al., 2002), which is above the maximum ceiling of the M-55 *Geophysica*. But, as shown here, until late March the refractory aerosol reaches down to the vortex bottom at about 400 K of potential temperature. Not only the mean large-scale subsidence inside the vortex, which more efficiently occurs at higher altitudes, but rather vertical dispersion may lead to the downward transport of refractory aerosol material into the lowermost vortex region, i.e. down to at least 400 K potential temperature. With the end of March the downward motion inside the Arctic vortex diminishes, and later the vortex dissolves, leaving the ingested material amenable for mixing towards mid latitudes. The vortex can thus be understood as a temporary stratospheric reservoir of refractory aerosol material imported from altitudes as high as the mesosphere.

When the vortex dissolves in early spring the particles are horizontally spreading towards mid-latitudes over the complete vertical extension of the former vortex. Over the following seasons, until a new vortex can form, a certain fraction of these particles may remain in the region above the Pole and will thus be incorporated in the newly forming vortex, descending to its lowermost part (between 400 and 500 K potential temperature) ahead of the newly incoming mesospheric air during early winter. Indeed our observations made during ESSenCE likely represent the lower vortex in just this state before additional fresh mesospheric refractory particles arrive from aloft. Assuming the simulation of Plumb et al., 2002 to be realistic we estimate that at the end of the Arctic winter about 10–20 % of the mesospheric air mass contributing to the whole vortex volume resides in the measurement region below 470 K (see Fig. 6 in Plumb et al., 2002).

ACPD
14, 9849–9901, 2014

Hence about the same fraction, at most about 30 % (considering the air mass to be twice as large in the column 67 to 1 hPa as in the observed column 100 to 67 hPa and assuming at least the same mean particle mixing ratio in the upper column), should be the visible part of the iceberg of refractory aerosol imported into the whole vortex. Assuming that the increase in the observed particle mass between 100 and 67 hPa from mid December to late winter (for instance the 32×10^6 kg for RECONCILE) can be largely attributed to fresh mesospheric particles, and that outflow of these particles at the vortex bottom is negligible (compared to the import from aloft), one would thus infer an import of mesospheric particles into the whole vortex of about 107×10^6 kg to 320×10^6 kg (from division of 32×10^6 kg by 0.3 and 0.1) for the RECONCILE winter 2009/2010.

The expected global daily influx of meteoritic material ranges at about 110×10^3 kg per day (Love and Brownlee, 1993). Thus up to 40×10^6 kg of meteoritic material may be deposed in the mesosphere per year. Assuming a steady state situation and symmetry between the two hemispheres, each polar vortex would remove half of this yearly influx over the course of a winter, i.e. 20×10^6 kg. Our estimate of total particle import from the mesosphere based on refractory aerosol masses in the lower vortex during early and late winter is thus a factor of about 5–16 higher than expected based on the daily influx of meteoritic material. This discrepancy on the one hand is well covered by the range of our estimate with factors of 0.05 to about 13 from the extreme maximum to the minimum of the involved uncertainties (cf. Table 3, data from RECONCILE and ESSenCe). On the other hand the remnants of refractory aerosols, which descended during previous winter season and which possibly persisted to some extent in the polar upper stratosphere until the next winter vortex starts forming, contribute also to the observed particle mass increase between 100 hPa und 67 hPa. Finally it remains open to further investigation if parts of the refractory aerosol in the Arctic vortex originate from sources other than the meteoritic influx into the mesosphere. In this sense our estimations only can provide some (highly uncertain) upper limit as we always assumed the observed refractory matter to be solely of meteoric origin.

ACPD
14, 9849–9901, 2014

6 Summary and conclusions

Inside the Arctic vortex up to 8 of 11 particles with diameters larger than 10 nm and smaller than a few µm were observed to consist of non-volatile material. During three Arctic winter seasons of the years 2003, 2010 and 2011 this observation was repeatedly made in qualitative agreement. This leads to the conclusion that the import of refractory aerosol material in the Arctic polar winter is a regular feature. We surmise that earlier observations of increased aerosol number concentration inside the Arctic vortex (Wilson et al., 1990; Hofmann et al., 1990) also comprise refractory aerosol and that new particle formation by homogeneous nucleation at the considered high altitudes plays a less crucial role than previously thought.

The quantity of refractory aerosols inside the vortex is connected to the transport history of air masses entering the vortex upper boundary from aloft which includes air that could originate from high as the lower mesosphere. Particle mixing ratios (up to 150 of non-volatile particles per milligram air) and the fraction of non-volatile particles (up to 75 %) are highest, if the air mass content of nitrous oxide (N_2O) is lowest (here down to 70 nmol mol^{-1}). The largest amounts of refractory aerosol inside the vortex appear in late winter (March), while in early winter (December) the import strength from upper stratospheric or mesospheric altitudes seems not to be fully developed, yet.

The abundance of refractory aerosol in the winter vortex is significantly driven by (a) the source strength (ablation of penetrating meteorites, volcanic activity, etc.) for the aerosol material, (b) the transport mechanism leading to long range advection at high altitudes in the stratosphere or mesosphere, (c) the vortex strength that induces the downwelling of air from these high altitudes, and (d) the vortex stability, as disturbances like vortex break up and mid-winter stratospheric warming enable air mass exchange across the vortex boundary and dilution with air from lower latitudes.

It can be assumed that the import of refractory aerosol likewise occurs due to the winter vortex subsidence also in the Antarctic. The extrapolation of our measurements

ACPD
14, 9849–9901, 2014

to a total aerosol mass in the lowermost vortex region (for pressure altitudes between 100 and 67 hPa) provides an estimate of the possible aerosol mass imported from aloft throughout an Arctic winter between early (ESSenCe) and late winter (RECONCILE). The resulting value is about 32×10^6 kg, which is a factor of 5.5 higher in comparison to early winter conditions. Related to the assumed influx of meteoritic aerosol material this estimate implies that the RECONCILE vortex might have included 5 to 16 times the mass of refractory aerosol that is expected to be deposed in the mesosphere by meteorites over the recent half-year. Large uncertainties of course are inherent in this approach. However, the value for the daily influx of meteoritic material still is a matter of debate, and the discrepancy between our estimate and the expectation is in fact more than covered by these uncertainties. Also contributions to the refractory aerosol mass from sources other than meteoritic influx and ablation may not be excluded.

One of the largest remaining unknowns is the chemical composition, the morphology, and physical nature of the refractory particles entering the polar vortex to unambiguously specify their origin. The amount and role of anthropogenic components from space debris, rocket launches and exhaust of high flying aircraft is not quantified well enough. Even contributions of soil materials continuously released by sub-Pinatubo volcanism (e.g. Souffriere Hills, Nabro, etc.) and other ground sources (like biomass burning) possibly need to be considered. Knowledge of the aerosol properties also is essential for conclusions concerning the particle sources as well as their role and effectiveness in PSC and cirrus cloud formation. Besides the need for more in situ measurements at high altitudes we emphasize the importance of laboratory experiments on heterogeneous nucleation of PSCs (particularly for NAT) on the observed refractory materials including particles coated with H_2SO_4, HNO_3, H_2O, and possibly other condensable materials.

Acknowledgements. The contributions from the technical staff at the workshops of the MPI for Chemistry and the Institute for Physics of the Atmosphere (Mainz University), as well as the Myasishchev Design Bureau (MDB) were crucial and essential. In particular we acknowledge support of T. Böttger, M. Flanz and W. Schneider. We very much thank the MDB

ACPD
14, 9849–9901, 2014

crew and the M55-*Geophysica* pilots. ESSenCe was in parts supported by the German Research Foundation (DFG) under contract HALO-SPP 1294/GR 3786. Some of our research leading to the presented results received funding from the European Research Council under the European Union's Seventh Framework Program (FP/2007-2013)/ERC Grant Agreement no. 321040 (EXCATRO). RECONCILE was supported by ESA, BMBF, and the EU (contract RECONCILE-226365-FP7-ENV-2008-1). Further financial support was provided by internal sources of the Johannes-Gutenberg University and the Max-Planck-Institute for Chemistry in Mainz, as well as the Karslruhe Institute for Technology and Forschungszentrum Jülich GmbH (both for ESSenCe). We dedicate this publication to our colleague and friend, C. Schiller, who was involved in EUPLEX and RECONCILE, and who passed away so untimely on 3 March 2012.

References

Biermann, U. M., Presper, T., Koop, T., Mossinger, J., Crutzen, P. J., and Peter, T.: The unsuitability of meteoritic and other nuclei for polar stratospheric cloud freezing, Geophys. Res. Lett., 23, 1693–1696, doi:10.1029/96gl01577, 1996.

Borrmann, S., Dye, J. E., Baumgardner, D., Proffitt, M. H., Margitan, J. J., Wilson, J. C., Jonsson, H. H., Brock, C. A., Loewenstein, M., Podolske, J. R., and Ferry, G. V.: Aerosols as dynamical tracers in the lower stratosphere – ozone versus aerosol correlation after the Mount-Pinatubo eruption, J. Geophys. Res.-Atmos., 100, 11147–11156, doi:10.1029/95jd00016, 1995.

Borrmann, S., Thomas, A., Rudakov, V., Yushkov, V., Lepuchov, B., Deshler, T., Vinnichenko, N., Khattatov, V., and Stefanutti, L.: Stratospheric aerosol measurements in the Arctic winter of 1996/1997 with the M-55 Geophysika high-altitude research aircraft, Tellus B, 52, 1088–1103, doi:10.1034/j.1600-0889.2000.00100.x, 2000.

Borrmann, S., Kunkel, D., Weigel, R., Minikin, A., Deshler, T., Wilson, J. C., Curtius, J., Volk, C. M., Homan, C. D., Ulanovsky, A., Ravegnani, F., Viciani, S., Shur, G. N., Belyaev, G. V., Law, K. S., and Cairo, F.: Aerosols in the tropical and subtropical UT/LS: in-situ measurements of submicron particle abundance and volatility, Atmos. Chem. Phys., 10, 5573–5592, doi:10.5194/acp-10-5573-2010, 2010.

ACPD
14, 9849–9901, 2014

Curtius, J., Weigel, R., Vössing, H.-J., Wernli, H., Werner, A., Volk, C.-M., Konopka, P., Krebsbach, M., Schiller, C., Roiger, A., Schlager, H., Dreiling, V., and Borrmann, S.: Observations of meteoric material and implications for aerosol nucleation in the winter Arctic lower stratosphere derived from in situ particle measurements, Atmos. Chem. Phys., 5, 3053–3069, doi:10.5194/acp-5-3053-2005, 2005.

Cziczo, D. J., Thomson, D. S., and Murphy, D. M.: Ablation, flux, and atmospheric implications of meteors inferred from stratospheric aerosol, Science, 291, 1772–1775, 2001.

Deshler, T.: A review of global stratospheric aerosol: measurements, importance, life cycle, and local stratospheric aerosol, Atmos. Res., 90, 223–232, doi:10.1016/j.atmosres.2008.03.016, 2008.

Dörnbrack, A., Pitts, M. C., Poole, L. R., Orsolini, Y. J., Nishii, K., and Nakamura, H.: The 2009–2010 Arctic stratospheric winter – general evolution, mountain waves and predictability of an operational weather forecast model, Atmos. Chem. Phys., 12, 3659–3675, doi:10.5194/acp-12-3659-2012, 2012.

Engel, A., Möbius, T., Haase, H.-P., Bönisch, H., Wetter, T., Schmidt, U., Levin, I., Reddmann, T., Oelhaf, H., Wetzel, G., Grunow, K., Huret, N., and Pirre, M.: Observation of mesospheric air inside the arctic stratospheric polar vortex in early 2003, Atmos. Chem. Phys., 6, 267–282, doi:10.5194/acp-6-267-2006, 2006.

Engel, I., Luo, B. P., Pitts, M. C., Poole, L. R., Hoyle, C. R., Grooß, J.-U., Dörnbrack, A., and Peter, T.: Heterogeneous formation of polar stratospheric clouds – Part 2: Nucleation of ice on synoptic scales, Atmos. Chem. Phys., 13, 10769–10785, doi:10.5194/acp-13-10769-2013, 2013.

Fahey, D. W., Kelly, K. K., Kawa, S. R., Tuck, A. F., Loewenstein, M., Chan, K. R., and Heidt, L. E.: Observations of denitrification and dehydration in the winter polar stratospheres, Nature, 344, 321–324, doi:10.1038/344321a0, 1990.

Fisher, M., O'Neill, A., and Sutton, R.: Rapid descent of mesospheric air into the stratospheric polar vortex, Geophys. Res. Lett., 20, 1267–1270, doi:10.1029/93gl01104, 1993.

Frey, W., Borrmann, S., Kunkel, D., Weigel, R., de Reus, M., Schlager, H., Roiger, A., Voigt, C., Hoor, P., Curtius, J., Krämer, M., Schiller, C., Volk, C. M., Homan, C. D., Fierli, F., Di Donfrancesco, G., Ulanovsky, A., Ravegnani, F., Sitnikov, N. M., Viciani, S., D'Amato, F., Shur, G. N., Belyaev, G. V., Law, K. S., and Cairo, F.: In situ measurements of tropical cloud properties in the West African Monsoon: upper tropospheric ice clouds, Mesoscale

ACPD
14, 9849–9901, 2014

Convective System outflow, and subvisual cirrus, Atmos. Chem. Phys., 11, 5569–5590, doi:10.5194/acp-11-5569-2011, 2011.
Gabrielli, P., Barbante, C., Plane, J. M. C., Varga, A., Hong, S., Cozzi, G., Gaspari, V., Planchon, F. A. M., Cairns, W., Ferrari, C., Crutzen, P., Cescon, P., and Boutron, C. F.: Meteoric smoke fallout over the Holocene epoch revealed by iridium and platinum in Greenland ice, Nature, 432, 1011–1014, doi:10.1038/Nature03137, 2004.
Grooß, J.-U., Engel, I., Borrmann, S., Frey, W., Günther, G., Hoyle, C. R., Kivi, R., Luo, B. P., Molleker, S., Peter, T., Pitts, M. C., Schlager, H., Stiller, G., Vömel, H., Walker, K. A., and Müller, R.: Nitric acid trihydrate nucleation and denitrification in the Arctic stratosphere, Atmos. Chem. Phys., 14, 1055–1073, doi:10.5194/acp-14-1055-2014, 2014.
Günther, G., Müller, R., von Hobe, M., Stroh, F., Konopka, P., and Volk, C. M.: Quantification of transport across the boundary of the lower stratospheric vortex during Arctic winter 2002/2003, Atmos. Chem. Phys., 8, 3655–3670, doi:10.5194/acp-8-3655-2008, 2008.
Haynes, P. and Shuckburgh, E.: Effective diffusivity as a diagnostic of atmospheric transport: 1. Stratosphere, J. Geophys. Res.-Atmos., 105, 22777–22794, doi:10.1029/2000jd900093, 2000.
Hofmann, D. J., Deshler, T., Arnold, F., and Schlager, H.: Balloon observations of nitric-acid aerosol formation in the Arctic stratosphere. 2. Aerosol, Geophys. Res. Lett., 17, 1279–1282, doi:10.1029/Gl017i009p01279, 1990.
Homan, C. D., Volk, C. M., Kuhn, A. C., Werner, A., Baehr, J., Viciani, S., Ulanovski, A., and Ravegnani, F.: Tracer measurements in the tropical tropopause layer during the AMMA/SCOUT-O3 aircraft campaign, Atmos. Chem. Phys., 10, 3615–3627, doi:10.5194/acp-10-3615-2010, 2010.
Hösen, E., Volk, C. M., Grooß, J.-U., Günther, G., and Werner, A.: The vortex index: an empirical origin of air tracer based on long-lived tracer measurements, Atmos. Chem. Phys., in preparation, 2014.
Hoyle, C. R., Engel, I., Luo, B. P., Pitts, M. C., Poole, L. R., Grooß, J.-U., and Peter, T.: Heterogeneous formation of polar stratospheric clouds – Part 1: Nucleation of nitric acid trihydrate (NAT), Atmos. Chem. Phys., 13, 9577–9595, doi:10.5194/acp-13-9577-2013, 2013.
Hunten, D. M., Turco, R. P., and Toon, O. B.: Smoke and dust particles of meteoric origin in the mesosphere and stratosphere, J. Atmos. Sci., 37, 1342–1357, 1980.
Jaenicke, R.: Atmospheric aerosols and global climate, J. Aerosol Sci., 11, 577–588, doi:10.1016/0021-8502(80)90131-7, 1980.

ACPD
14, 9849–9901, 2014

Jones, J. and Kaiser, T. R.: The effects of thermal radiation, conduction and metoriod heat capacity on meteoric ablation, Mon. Not. R. Astron. Soc., 133, 411–420, 1966.

Kaufmann, M., Blank, J., Guggenmoser, T., Ungermann, J., Engel, A., Ern, M., Friedl-Vallon, F., Gerber, D., Grooss, J.-U., Günther, G., Höpfner, M., Kleinert, A., Latzko, T., Maucher, G., Neubert, T., Nordmeyer, H., Oelhaf, H., Olschewski, F., Orphal, J., Preusse, P., Schlager, H., Schneider, H., Schuettemeyer, D., Stroh, F., Suminska-Ebersoldt, O., Vogel, B., Volk, M., Wintel, J., Woiwode, W., and Riese, M.: Retrieval of three-dimensional small scale structures in upper tropospheric/lower stratospheric composition as measured by GLORIA, Atmos. Meas. Tech. Discuss., in press, 2014.

Konopka, P., Günther, G., Müller, R., dos Santos, F. H. S., Schiller, C., Ravegnani, F., Ulanovsky, A., Schlager, H., Volk, C. M., Viciani, S., Pan, L. L., McKenna, D.-S., and Riese, M.: Contribution of mixing to upward transport across the tropical tropopause layer (TTL), Atmos. Chem. Phys., 7, 3285–3308, doi:10.5194/acp-7-3285-2007, 2007.

Love, S. G. and Brownlee, D. E.: A direct measurement of the terrestrial mass accretion rate of cosmic dust, Science, 262, 550–553, doi:10.1126/science.262.5133.550, 1993.

Mann, G.W., Davies, S., Carslaw, K. S., and Chipperfield, M. P.: Factors controlling Arctic denitrification in cold winters of the 1990s, Atmos. Chem. Phys., 3, 403–416, doi:10.5194/acp-3-403-2003, 2003.

McKenna, D. S., Grooß, J.-U., Günther, G., Konopka, P., Müller, R., Carver, G., and Sasano, Y.: A new Chemical Lagrangian Model of the Stratosphere (CLaMS) 2. Formulation of chemistry scheme and initialization, J. Geophys. Res.-Atmos., 107, ACH 4-1–ACH 4-14, doi:10.1029/2000jd000113, 2002a.

McKenna, D. S., Konopka, P., Grooß, J.-U., Günther, G., Müller, R., Spang, R., Offermann, D., and Orsolini, Y.: A new Chemical Lagrangian Model of the Stratosphere (CLaMS) 1. Formulation of advection and mixing, J. Geophys. Res.-Atmos., 107, ACH 15-11–ACH 15-15, doi:10.1029/2000jd000114, 2002b.

Molleker, S., Borrmann, S., Schlager, H., Luo, B., Frey, W., Klingebiel, M., Weigel, R., Ebert, M., Mitev, V., Matthey, R., Peter, T., Woiwode, W., Dörnbrack, A., Günther, G., Vogel, B., Grooß, J.-U., Spelten, N., and Cairo, F.: Microphysical properties of synoptic scale polar stratospheric clouds: in-situ measurements of unexpectedly large HNO_3 containing particles in the Arctic vortex, Atmos. Chem. Phys. Discuss., submitted, 2014.

Murphy, C.: Just and unjust peace: an ethic of political reconciliation, Ethics, 123, 577–581, doi:10.1086/670363, 2013.

ACPD
14, 9849–9901, 2014

Peter, T.: Microphysics and heterogeneous chemistry of polar stratospheric clouds, Annu. Rev. Phys. Chem., 48, 785–822, doi:10.1146/annurev.physchem.48.1.785, 1997.
Peter, T. and Grooß, J.-U.: Chapter 4, Polar stratospheric clouds and sulfate aerosol particles: microphysics, denitrification and heterogeneous chemistry, in: Stratospheric Ozone Depletion and Climate Change, The Royal Society of Chemistry, Cambridge, UK, 108–144, 2012.
Peucker-Ehrenbrink, B.: Accretion of extraterrestrial matter during the last 80 million years and its effect on the marine osmium isotope record, Geochim. Cosmochim. Ac., 60, 3187–3196, doi:10.1016/0016-7037(96)00161-5, 1996.
Plane, J. M. C.: A time-resolved model of the mesospheric Na layer: constraints on the meteor input function, Atmos. Chem. Phys., 4, 627–638, doi:10.5194/acp-4-627-2004, 2004.
Plumb, R. A.: Tracer interrelationships in the stratosphere, Rev. Geophys., 45, RG4005, doi:10.1029/2005RG000179, 2007.
Plumb, R. A., Heres, W., Neu, J. L., Mahowald, N. M., del Corral, J., Toon, G. C., Ray, E., Moore, F., and Andrews, A. E.: Global tracer modeling during SOLVE: high-latitude descent and mixing, J. Geophys. Res.-Atmos., 107, 8309, doi:10.1029/2001jd001023, 2002.
Prather, M. J. and Rodriguez, J. M.: Antarctic ozone: meteoric control of HNO_3, Geophys. Res. Lett., 15, 1–4, doi:10.1029/GL015i001p00001, 1988.
Randall, C. E., Harvey, V. L., Singleton, C. S., Bernath, P. F., Boone, C. D., and Kozyra, J. U.: Enhanced NO_x in 2006 linked to strong upper stratospheric Arctic vortex, Geophys. Res. Lett., 33, L18811, doi:10.1029/2006gl027160, 2006.
Rapp, M. and Strelnikova, I.: Measurements of meteor smoke particles during the ECOMA-2006 campaign: 1. Particle detection by active photoionization, J. Atmos. Sol.-Terr. Phy., 71, 477–485, doi:10.1016/j.jastp.2008.06.002, 2009.
Rapp, M., Strelnikova, I., and Gumbel, J.: Meteoric smoke particles: evidence from rocket and radar techniques, Adv. Space. Res., 40, 809–817, doi:10.1016/j.asr.2006.11.021, 2007.
Shur, G. N., Sitnikov, N. M., and Drynkov, A. V.: A mesoscale structure of meteorological fields in the tropopause layer and in the lower stratosphere over the southern tropics (Brazil), Russ. Meteorol. Hydrol., 32, 487–494, doi:10.3103/s106837390708002x, 2007.
Sokolov, L. and Lepuchov, B.: Protocol of Interaction Between Unit for Connection with Scientific Equipment (UCSE) and On-Board Scientific Equipment of Geophysica Aircraft, 2nd Edn., Myasishchev Design Bureau (MDB), Moscow, 1998.
Solomon, S.: Stratospheric ozone depletion: a review of concepts and history, Rev. Geophys., 37, 275–316, doi:10.1029/1999rg900008, 1999.

ACPD
14, 9849–9901, 2014

Spang, R., Stroh, F., von Hobe, M., Gerber, D., Moyna, B., Oldfield, M., Rea, S., Reburn, J., Siddans, R., Kerridge, B., Oelhaf, H., and Woiwode, W.: Data Acquisition Report of the PremierEX Scientific Flights, Final Report for ESTEC, Contract No. 2670/09/NL/CT "PREMIER Experiment", 3139, 3151, available at: https://earth.esa.int/documents/10174/87248/PremierEX_FinalReport_v2.pdf (last access: 25 May 2013), 2012.

Stefanutti, L., Sokolov, L., Balestri, S., MacKenzie, A. R., and Khattatov, V.: The M-55 Geophysica as a platform for the airborne polar experiment, J. Atmos. Ocean. Tech., 16, 1303–1312, doi:10.1175/1520-0426(1999)016<1303:tmgaap>2.0.co;2, 1999.

Strelnikova, I., Rapp, M., Strelnikov, B., Baumgarten, G., Brattli, A., Svenes, K., Hoppe, U. P., Friedrich, M., Gumbel, J., and Williams, B. P.: Measurements of meteor smoke particles during the ECOMA-2006 campaign: 2. Results, J. Atmos. Sol.-Terr. Phy., 71, 486–496, doi:10.1016/j.jastp.2008.07.011, 2009.

Vogel, B., Konopka, P., Grooß, J.-U., Müller, R., Funke, B., López-Puertas, M., Reddmann, T., Stiller, G., von Clarmann, T., and Riese, M.: Model simulations of stratospheric ozone loss caused by enhanced mesospheric NO_x during Arctic Winter 2003/2004, Atmos. Chem. Phys., 8, 5279–5293, doi:10.5194/acp-8-5279-2008, 2008.

Voigt, C., Schlager, H., Luo, B. P., Dörnbrack, A., Roiger, A., Stock, P., Curtius, J., Vössing, H., Borrmann, S., Davies, S., Konopka, P., Schiller, C., Shur, G., and Peter, T.: Nitric Acid Trihydrate (NAT) formation at low NAT supersaturation in Polar Stratospheric Clouds (PSCs), Atmos. Chem. Phys., 5, 1371–1380, doi:10.5194/acp-5-1371-2005, 2005.

von Hobe, M., Bekki, S., Borrmann, S., Cairo, F., D'Amato, F., Di Donfrancesco, G., Dörnbrack, A., Ebersoldt, A., Ebert, M., Emde, C., Engel, I., Ern, M., Frey, W., Genco, S., Griessbach, S., Grooß, J.-U., Gulde, T., Günther, G., Hösen, E., Hoffmann, L., Homonnai, V., Hoyle, C. R., Isaksen, I. S. A., Jackson, D. R., Jánosi, I. M., Jones, R. L., Kandler, K., Kalicinsky, C., Keil, A., Khaykin, S. M., Khosrawi, F., Kivi, R., Kuttippurath, J., Laube, J. C., Lefèvre, F., Lehmann, R., Ludmann, S., Luo, B. P., Marchand, M., Meyer, J., Mitev, V., Molleker, S., Müller, R., Oelhaf, H., Olschewski, F., Orsolini, Y., Peter, T., Pfeilsticker, K., Piesch, C., Pitts, M. C., Poole, L. R., Pope, F. D., Ravegnani, F., Rex, M., Riese, M., Röckmann, T., Rognerud, B., Roiger, A., Rolf, C., Santee, M. L., Scheibe, M., Schiller, C., Schlager, H., Siciliani de Cumis, M., Sitnikov, N., Søvde, O. A., Spang, R., Spelten, N., Stordal, F., Sumińska-Ebersoldt, O., Ulanovski, A., Ungermann, J., Viciani, S., Volk, C. M., vom Scheidt, M., von der Gathen, P., Walker, K., Wegner, T., Weigel, R., Weinbruch, S., Wetzel, G., Wienhold, F. G., Wohltmann, I., Woiwode, W., Young, I. A. K., Yushkov, V., Zobrist, B.,

ACPD
14, 9849–9901, 2014

and Stroh, F.: Reconciliation of essential process parameters for an enhanced predictability of Arctic stratospheric ozone loss and its climate interactions (RECONCILE): activities and results, Atmos. Chem. Phys., 13, 9233–9268, doi:10.5194/acp-13-9233-2013, 2013.

von Zahn, U.: The total mass flux of meteoroids into the Earth's upper atmosphere, in: 17th ESA Symposium on European Rocket and Balloon Programmes and Related Research, 30 May–2 June 2005, Sandefjord, Norway, edited by: B. Warmbein, ESA SP-590, ESA Publications Division, Noordwijk, ISBN 92-9092-901-4, 33–39, 2005.

Waibel, A. E., Peter, T., Carslaw, K. S., Oelhaf, H., Wetzel, G., Crutzen, P. J., Poschl, U., Tsias, A., Reimer, E., and Fischer, H.: Arctic ozone loss due to denitrification, Science, 283, 2064–2069, doi:10.1126/science.283.5410.2064, 1999.

Wang, P. H., McCormick, M. P., Swissler, T. J., Osborn, M. T., Fuller, W. H., and Yue, G. K.: Inference of stratospheric aerosol composition and size distribution from Sage-II satellite measurements, J. Geophys. Res.-Atmos., 94, 8435–8446, doi:10.1029/Jd094id06p08435, 1989.

Wegner, T., Grooß, J.-U., von Hobe, M., Stroh, F., Sumińska-Ebersoldt, O., Volk, C. M., Hösen, E., Mitev, V., Shur, G., and Müller, R.: Heterogeneous chlorine activation on stratospheric aerosols and clouds in the Arctic polar vortex, Atmos. Chem. Phys., 12, 11095–11106, doi:10.5194/acp-12-11095-2012, 2012.

Weigel, R., Hermann, M., Curtius, J., Voigt, C., Walter, S., Böttger, T., Lepukhov, B., Belyaev, G., and Borrmann, S.: Experimental characterization of the COndensation PArticle counting System for high altitude aircraft-borne application, Atmos. Meas. Tech., 2, 243–258, doi:10.5194/amt-2-243-2009, 2009.

Weigel, R., Borrmann, S., Kazil, J., Minikin, A., Stohl, A., Wilson, J. C., Reeves, J. M., Kunkel, D., de Reus, M., Frey, W., Lovejoy, E. R., Volk, C. M., Viciani, S., D'Amato, F., Schiller, C., Peter, T., Schlager, H., Cairo, F., Law, K. S., Shur, G. N., Belyaev, G. V., and Curtius, J.: In situ observations of new particle formation in the tropical upper troposphere: the role of clouds and the nucleation mechanism, Atmos. Chem. Phys., 11, 9983–10010, doi:10.5194/acp-11-9983-2011, 2011.

Weinheimer, A. J., Walega, J. G., Ridley, B. A., Sachse, G. W., Anderson, B. E., and Collins, J. E.: Stratospheric NO_y measurements on the Nasa Dc-8 during Aase-Ii, Geophys. Res. Lett., 20, 2563–2566, doi:10.1029/93gl02627, 1993.

ACPD
14, 9849–9901, 2014

Werner, A., Volk, C. M., Ivanova, E. V., Wetter, T., Schiller, C., Schlager, H., and Konopka, P.: Quantifying transport into the Arctic lowermost stratosphere, Atmos. Chem. Phys., 10, 11623–11639, doi:10.5194/acp-10-11623-2010, 2010.

Wilson, J. C., Stolzenburg, M. R., Clark, W. E., Loewenstein, M., Ferry, G. V., and Chan, K. R.: Measurements of condensation nuclei in the airborne arctic stratospheric expedition – observations of particle-production in the polar vortex, Geophys. Res. Lett., 17, 361–364, doi:10.1029/Gl017i004p00361, 1990.

Woiwode, W., Grooß, J.-U., Oelhaf, H., Molleker, S., Borrmann, S., Ebersoldt, A., Frey, W., Gulde, T., Khaykin, S., Maucher, G., Piesch, C., and Orphal, J.: Denitrification by large NAT particles: the impact of reduced settling velocities and hints on particle characteristics, Atmos. Chem. Phys. Discuss., 14, 5893–5927, doi:10.5194/acpd-14-5893-2014, 2014.

ACPD
14, 9849–9901, 2014

Table 1. Parameterization of the linear regression between the particle mixing ratio N_{10}nv with potential temperature Θ and with N_2O mixing ratio for different altitude ranges, Θ < 410 K and Θ > 410 K, respectively, within the vortex as displayed in Fig. 8. $y = f(x) = ax + b$ in mg^{-1}; a_1, b_1 and correlation coefficient r_1^2 for 390 K < Θ ≤ 410 K; a_2, b_2 and correlation coefficient r_2^2 for Θ > 410 K.

	with x = Θ in K			with x = N_2O in nmol mol^{-1}		
	EUPLEX	RECONCILE	ESSenCe	EUPLEX	RECONCILE	ESSenCe
a_1	–	0.34 ± 0.02	0.42 ± 0.06	–	−0.21 ± 0.02	−0.19 ± 0.04
b_1	–	−96.3 ± 7.5	−135.6 ± 24.8	–	88.3 ± 3.9	77.3 ± 9.2
r_1^2	–	0.43	0.52	–	0.45	0.58
a_2	1.01 ± 0.02	1.56 ± 0.01	0.54 ± 0.02	−0.71 ± 0.05	−0.68 ± 0.01	−0.21 ± 0.01
b_2	−365.8 ± 8.9	−616.3 ± 5.3	−187.9 ± 9.3	178.5 ± 2.1	180.9 ± 1.1	81.4 ± 1.2
r_2^2	0.74	0.83	0.54	0.85	0.90	0.72

ACPD
14, 9849–9901, 2014

Table 2. Estimated volume (v_p) of one refractory aerosol particle, particulate material density (ρ_p) and parameterized Θ-p-relationship for an extrapolation of the total mass of refractory aerosol within the Vortex volume (cf. Sect. 6).

	v_p in m^3	ρ_p in $kg\,m^{-3}$	p in hPa = $A + \exp(-C \cdot (\Theta \text{ in K} - B))$								
			EUPLEX			RECONCILE			ESSenCe		
			A	B	C	A	B	C	A	B	C
Mean	5.00×10^{-20}	1400	46.1	550.5	0.0252	39.3	698.6	0.0149	46.0	557.6	0.0246
Min	8.71×10^{-21}	1000	31.8	594.7	0.0198	34.3	743.4	0.0125	38.8	592.3	0.0203
Max	1.86×10^{-19}	2000	30.8	753.8	0.0127	25.1	832.7	0.0110	4.87	823.0	0.0109

ACPD
14, 9849–9901, 2014

Table 3. Averaged vortex cross section areas from CLaMS analyses and resulting altitude-resolved refractory aerosol mass as well as the integrated aerosol mass in the vortex, extrapolated from the in situ measurements under various assumptions (cf. Sect. 6). Vertical coordinates are provided as potential temperature and according pressure-range from the Θ-p functional relation provided in Table 2. With applying variation range factors the extremes of involved uncertainties are covered.

	averaged vortex cross section area in km^2			altitude resolved mass of refractory aerosol M_{nv}					
	EUPLEX	RECONCILE	ESSenCe	EUPLEX		RECONCILE		ESSenCe	
Θ in K				p range in hPa	M_{nv} in kg	p range in hPa	M_{nv} in kg	p range in hPa	M_{nv} in kg
400	–	12 873 600	6 437 790	–	–	131–119	4.7×10^6	101–89	1.8×10^6
410	10 259 900	15 007 800	7 474 930	85–77	3.1×10^6	119–108	5.1×10^6	89–79	1.7×10^6
420	13 184 650	16 898 750	9 309 220	77–70	3.7×10^6	108–98	4.5×10^6	79–72	1.9×10^6
430	15 466 600	18 565 200	11 463 200	70–64	4.0×10^6	98–90	5.9×10^6	72–66	2.1×10^6
440	16 893 950	20 123 350	13 472 600	64–60	3.9×10^6	90–83	7.1×10^6	66–62	2.1×10^6
450	18 023 400	21 159 700	14 218 900	60–57	3.6×10^6	83–77	7.9×10^6	62–58	2.0×10^6
460	19 140 750	22 579 350	14 915 600	57–55	3.4×10^6	77–72	8.6×10^6	58–56	1.8×10^6
470	20 157 300	23 282 300	–	55–53	3.0×10^6	72–67	8.8×10^6	–	–
480	21 287 700	–	–	53–51	2.7×10^6	–	–	–	–
490	22 248 850	–	–	51–50	2.4×10^6	–	–	–	–
500	23 147 150	–	–	50–49	2.1×10^6	–	–	–	–
				Summed mass of refractory aerosol in kg					
			total sum		32.0×10^6		52.5×10^6		13.3×10^6
			variation range factor (min.–max.)		0.07–21.0		0.05–12.6		0.06–15.4
			sum (100–67 hPa)		–		39.10×10^6		7.09×10^6
			variation range factor (min.–max.)		–		0.05–13.1		0.06–12.2

ACPD
14, 9849–9901, 2014

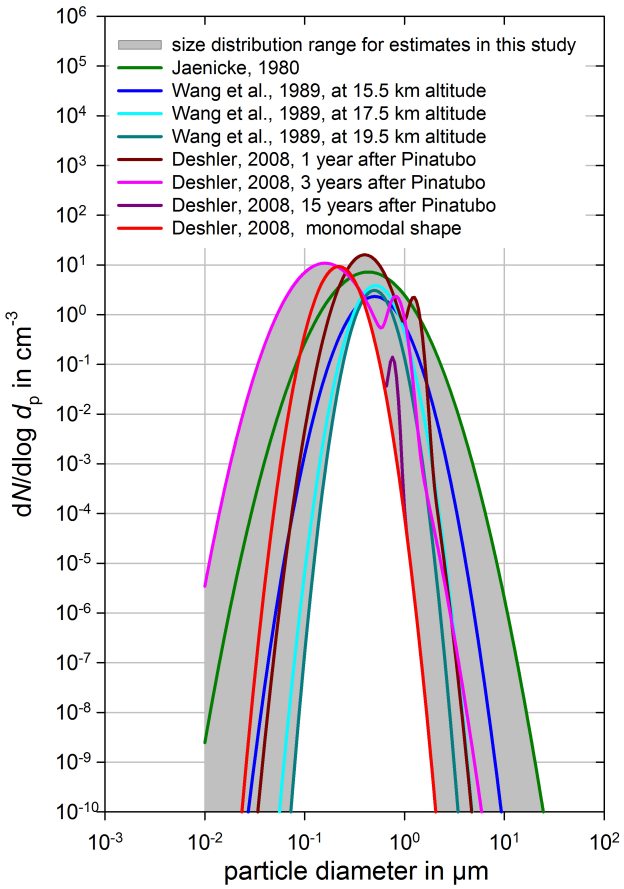

Fig. 1. Model size distributions of stratospheric aerosol as provided in parameterized form by three different sources: Jaenicke, 1980; Wang et al., 1989 and Deshler, 2008. The grey shaded area denotes the range from maximum to minimum values of the size distributions that are used for the estimates described in Sect. 5.

ACPD
14, 9849–9901, 2014

Enhanced refractory aerosol in the Arctic vortex

R. Weigel et al.

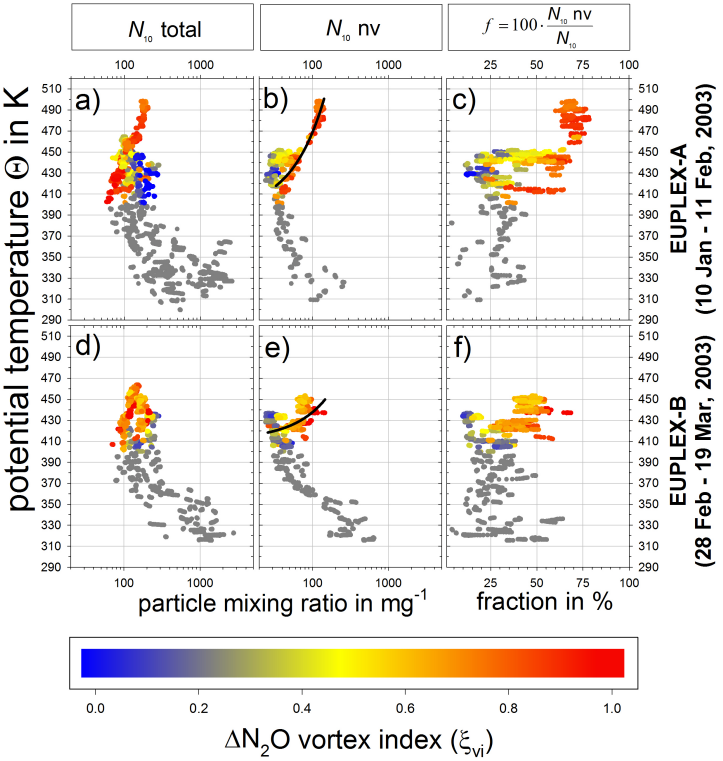

Fig. 2. Vertical distribution of particle mixing ratio N_{10} (left column), N_{10}nv (mid column) and resulting fraction f of non-volatile particles (right column) vs. the potential temperature Θ for the EUPLEX campaign in 2003. Data are additionally subdivided (cf. Sect. 3) in period A (January–February) and period B (February–March). Data points for Θ above 400 K color-coded according to ΔN_2O vortex index ξ_{vi}. For Θ below 400 K, data points are left in grey as inside or outside vortex apportioning is not unambiguous (cf. Sect. 2). Black lines indicate a regression over those data points which fulfill the inside-vortex criterion (Sect. 2).

ACPD
14, 9849–9901, 2014

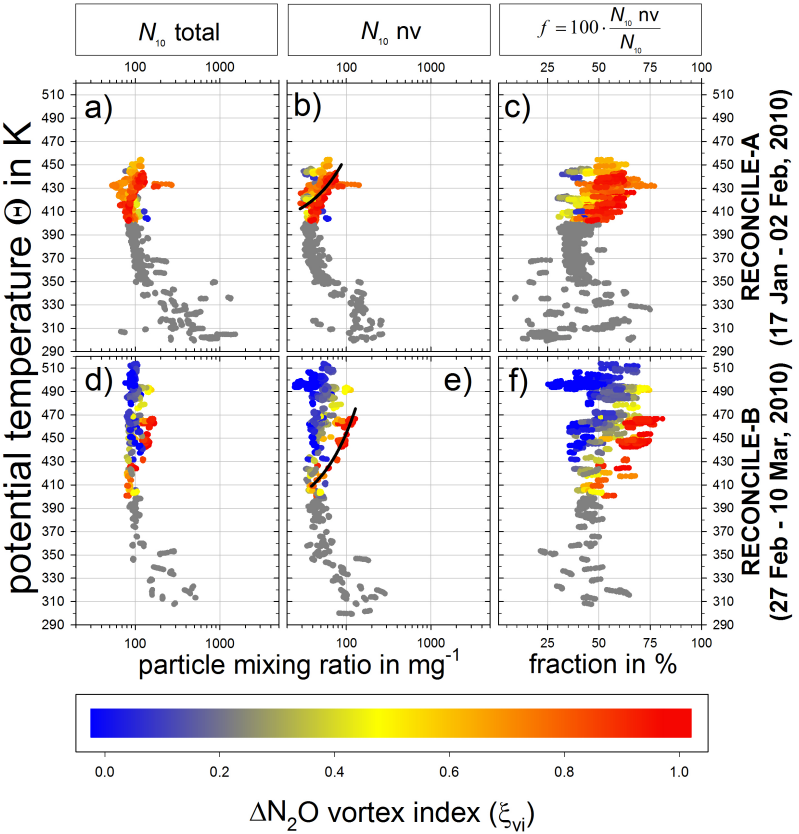

Fig. 3. Structured as Fig. 2 for the RECONCILE campaign in 2010 with a subdivision of the mission periods like for EUPLEX. Data are color-coded according to the ΔN_2O vortex index ξ_{vi}. For Θ below 400 K, data points are left in grey as the inside or outside vortex apportioning not unambiguous (cf. Sect. 2). Black lines indicate a regression of data points that fulfill the inside-vortex criterion (Sect. 2).

ACPD
14, 9849–9901, 2014

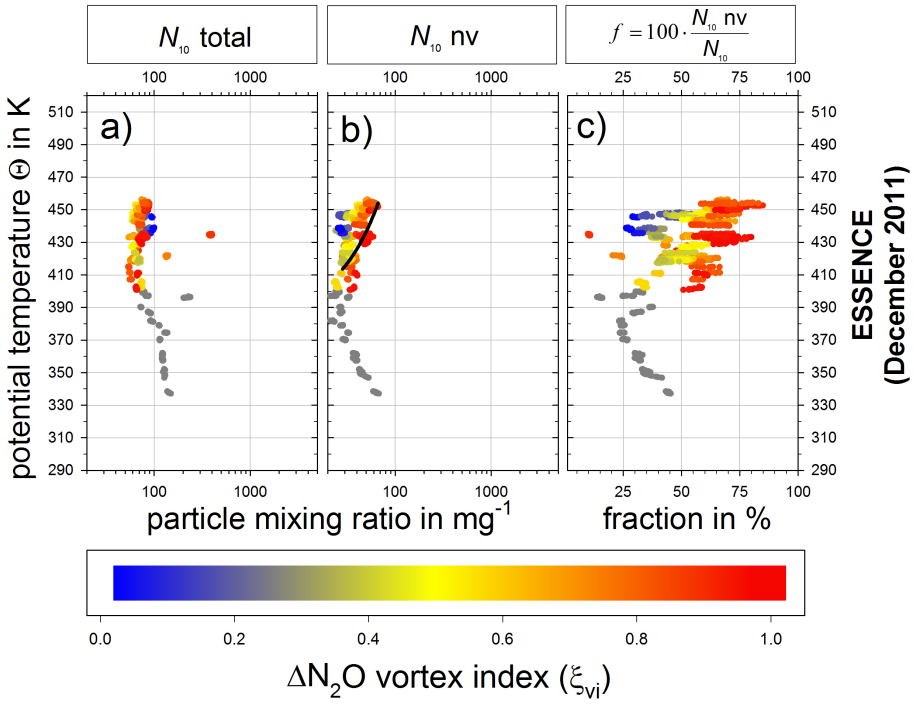

Fig. 4. Structured as Figs. 2 and 3 for the ESSenCE campaign in 2011 with the color-coding of data according to the ΔN_2O vortex index ξ_{vi}. For Θ below 400 K, data points are left in grey as inside or outside vortex apportioning not unambiguous (cf. Sect. 2). Black lines indicate a regression of data points that fulfill the inside-vortex criterion (Sect. 2).

ACPD
14, 9849–9901, 2014

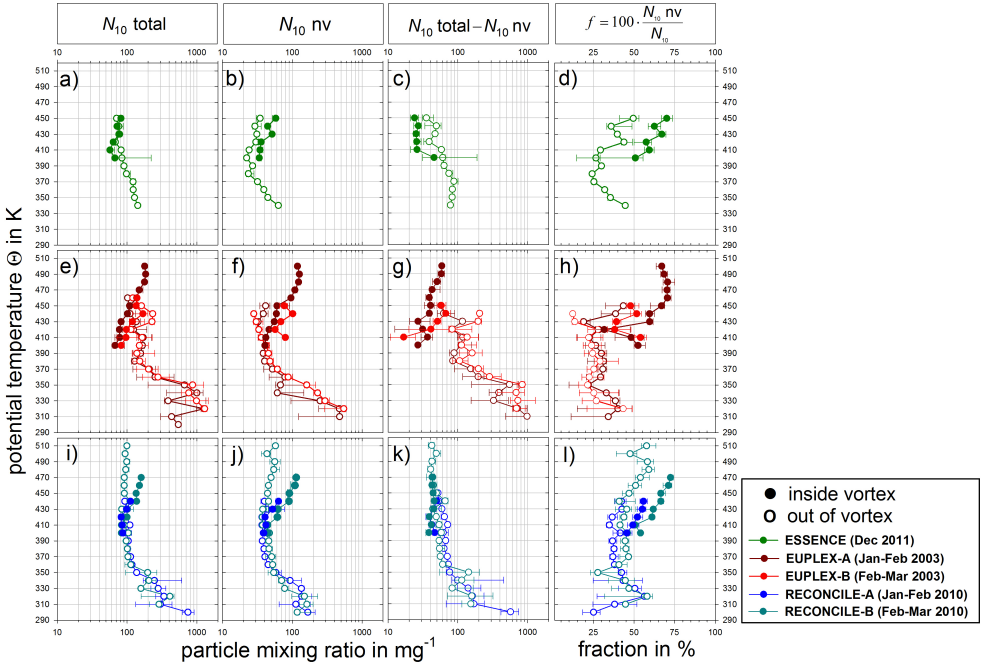

Fig. 5. Median vertical profiles of particle mixing ratios with 25- and 75-percentiles (bars) as function of potential temperature Θ. Data are attributed to either originate from inside (dots) or outside the vortex (circles) by using the ΔN_2O vortex index ξ_{vi} (cf. Sect. 2). Aerosol mixing ratios N_{10}, (left column), N_{10}nv (mid-left column), mixing ratio difference $N_{10} - N_{10}$nv (mid-right column) and resulting fraction f of refractory particles (right column). **(a–d)** from ESSenCe (i.e. the mission conducted the earliest in the winter season); **(e–h)** data from EUPLEX; **(i–l)** results from RECONCILE.

ACPD
14, 9849–9901, 2014

Enhanced refractory aerosol in the Arctic vortex

R. Weigel et al.

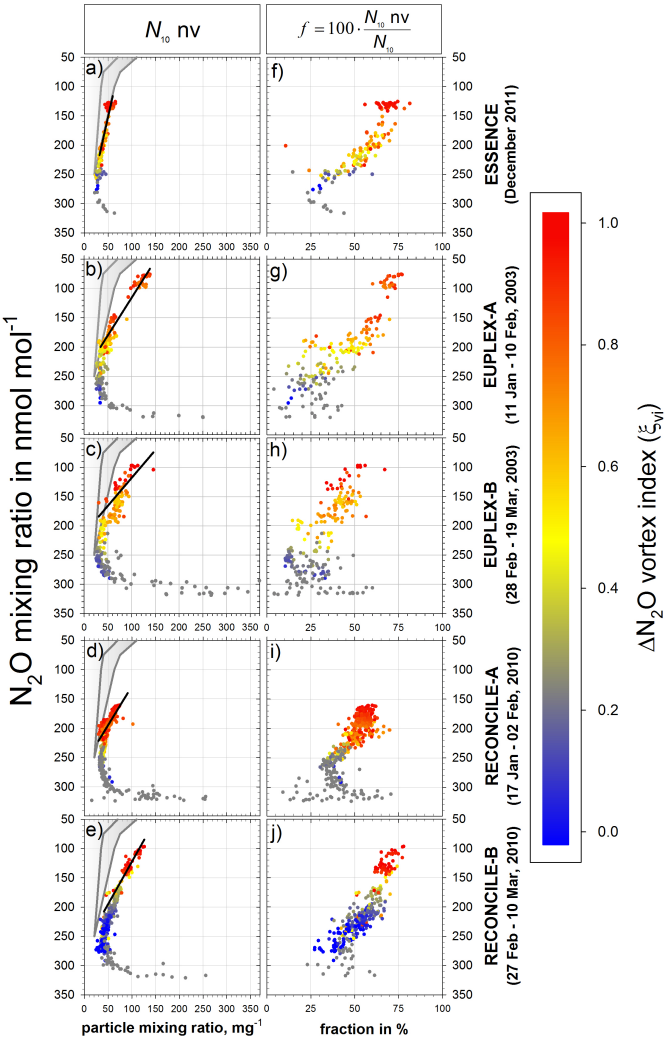

ACPD
14, 9849–9901, 2014

Enhanced refractory aerosol in the Arctic vortex

R. Weigel et al.

Fig. 6. Mixing ratio of non-volatile particles N_{10}nv and their fractional contribution f to measured total aerosol abundance as function of N_2O mixing ratio. The data points are colored according to the ΔN_2O vortex index ξ_{vi} or are designated in grey if measurements occurred at Θ levels below 400 K for which inside or outside vortex apportioning is not unambiguous (cf. Sect. 2). For data measured inside the vortex ($\xi_{vi} > 0.75$) the black lines indicate a linear correlation. Alternatively, for N_2O below 250 nmol mol^{-1}, the course of canonical curves within plausible limits are implied as grey lines with the ESSenCe data (early winter) as the uppermost limit **(a)**. The same early–winter climatology provides a reference for comparison to data from measurements in progressed winter **(b–e)**.

ACPD
14, 9849–9901, 2014

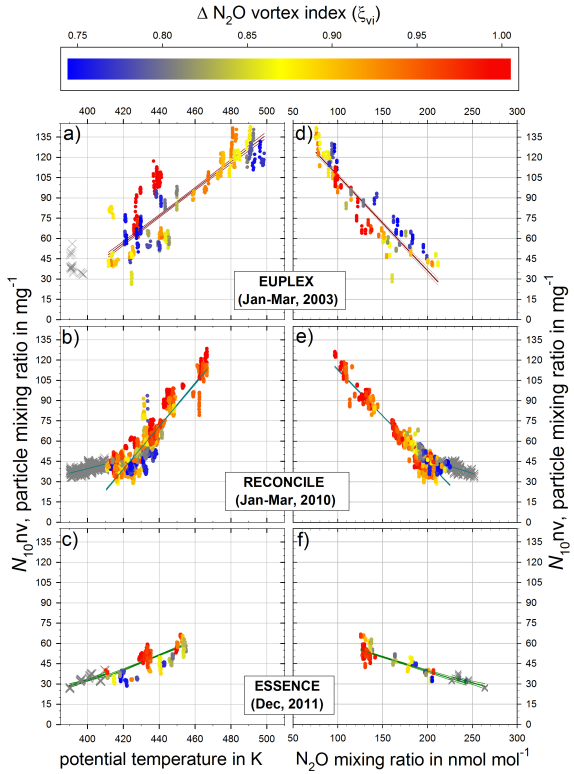

Fig. 7. Mixing ratio of non-volatile particles N_{10}nv as function of potential temperature Θ **(a–c)** and N_2O mixing ratio **(d–f)** for measurements in the vortex (i.e. where ΔN_2O vortex index $\xi_{vi} > 0.75$). Data points are colored by means of ΔN_2O vortex index in the range $0.75 < \xi_{vi} < 1$. Results are separated for Θ levels below 410 K (crosses) and above 410 K (dots) to account for the visible discontinuity, a transition zone at the vortex bottom. Linear correlations are assumed for Θ levels above 410 K and linear regressions with 95 % confidence interval are implied. These are separately displayed in Fig. 8 for better comparability.

ACPD
14, 9849–9901, 2014

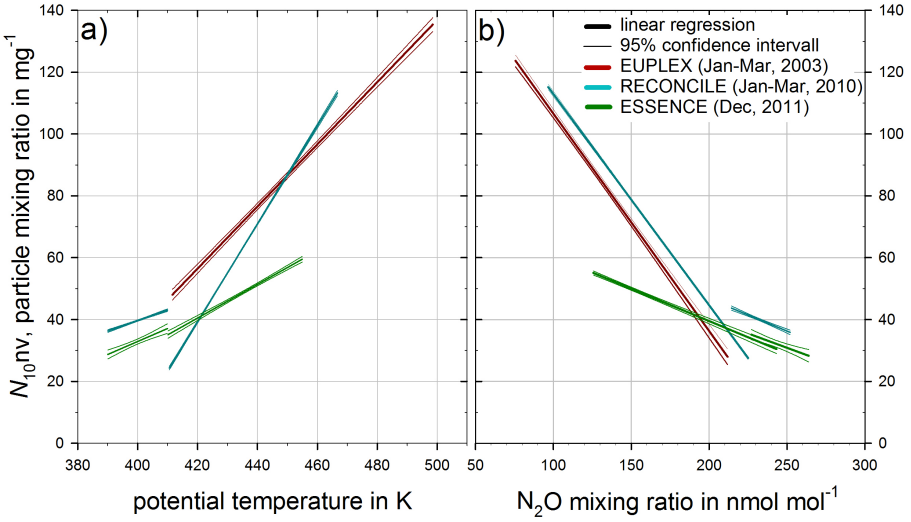

Fig. 8. Linear regressions with 95 % confidence interval for the mixing ratio of non-volatile particles N_{10}nv as function of potential temperature Θ **(a)** and N_2O mixing ratio **(b)**. Results from measurements within the vortex (ΔN_2O vortex index $\xi_{vi} > 0.75$) are shown of the three Arctic missions: EUPLEX (2003), RECONCILE (2010) and ESSenCe (2011).

ACPD
14, 9849–9901, 2014